BULLETIN OF THE EARTHQUAKE
RESEARCH INSTITUTE
Vol. 47 (1969), pp. 487-521

21. A Long Wave in the Vicinity of an Estuary [VI].

By Takao MOMOI,
Earthquake Research Institute.

(Read March 25, 1969.—Received March 30, 1969.)

Abstract

In this paper, the long waves around the estuary are discussed for the RST wave in Section 3, the RD wave in Section 4, the secondary reflection in Section 5, the effect of the canal in Section 6, the effect of the corner of the estuary upon the diffracted wave from the other corner in Section 7, and the emitting point of the RD wave in Section 9. And further the secondary reflection of the diffracted wave around the single right-angled corner at the leeward coast is examined in Section 8.

The conspicuous features exposed are as follows.

(i) The lateral mode in the canal of the estuary is the greatest in intensity for $kd=\pi$ (k: the wave number of the incident wave, d: the half width of the canal), the value of which amounts to about 0.5 (the amplitude of the incident wave is assumed as 1.0).

(ii) When kd is small, the secondary reflection of the diffracted waves around the estuary are composed of two kinds of waves. One is the secondary reflection along the coast near the mouth of the estuary, directing to the open sea, and the other that along the bank of the canal near the mouth which is directed toward the inside of the canal.

(iii) Among the secondarily reflected waves of the diffracted waves around the estuary, the secondary reflection from the bank of the canal directly behind the coast, in which the invading wave is diffracted toward the inside of the canal, is in intensity about four or five times the other secondary reflections.

1. Introduction

The present work is a continuation of the previous works (*Momoi*, 1965a, 1965b, 1966, 1968a and 1968b) concerning the long wave around the estuary.

2. The Model Used and the Theory

The model used in the present work is completely the same as that in the previous works (*Momoi*, 1965a–1968b). For the model, the reader

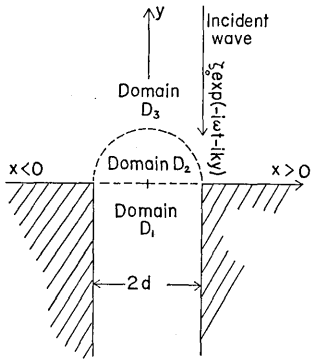

Fig. 1. Geometry of the model used.

should refer to Fig. 1. The definitions and the notations used are exactly the same as those in the previous works, unless otherwise stated. The theory and the computation technique go along the same lines as those described in Section 2 of the last paper (*Momoi*, 1968b).

3. RST Wave

Amplitude and Phase of the RST Wave.

The further calculation of the RST (resultant) wave is made up to $kd=4.0$ from 3.05 (k: the wave number of the incident wave, d: the half width of the canal), the results of which are shown in Figs. 2a(p) to 9a(p). Figs. 2a to 9a showing the amplitude variation reveals that the lateral oscillation inside the canal is the most dominant for $kd=3.15$ ($\fallingdotseq\pi$), the value of which amount to about 1.5 in wave height. On inspection of the figures concerning the phase variation (Figs. 2p to 9p), the following are found. The crest line of phase zero at the mouth of the canal runs diverting to the side of the open sea near the corner of the estuary, while that in the case of the double breakwater wings is found to run rigidly along the breakwater gap from equation (33) of the first paper concerning the long wave around the breakwater (*Momoi*, 1967a) (see Fig. 10). The above diversion (retardation) in the case of the estuary is caused by two kinds of the waves. The first of the waves is the reflection of the diffracted wave around the corner toward the open sea from the bank of the canal and the second is the secondary reflection of the diffracted wave, from the other corner, at the corner of the estuary to the open sea (see Fig. 11). For the first of the above-mentioned waves, the reader should refer to Section 8 (Reflection of the Diffracted Wave around the Right-angled Corner).

In Fig. 12, the convergence check is made through the calculations of the amplitude of the RST wave under the fifteenth and seventeenth approximations. The above figure denotes that the agreement of two approximations is good enough to discuss the behavior of the wave around the estuary.

Agreement with the Solution of Mirror Image.

The approximated theory by the method of mirror image has been developed in Section 7 of the fifth paper (*Momoi*, 1968b). The agreement

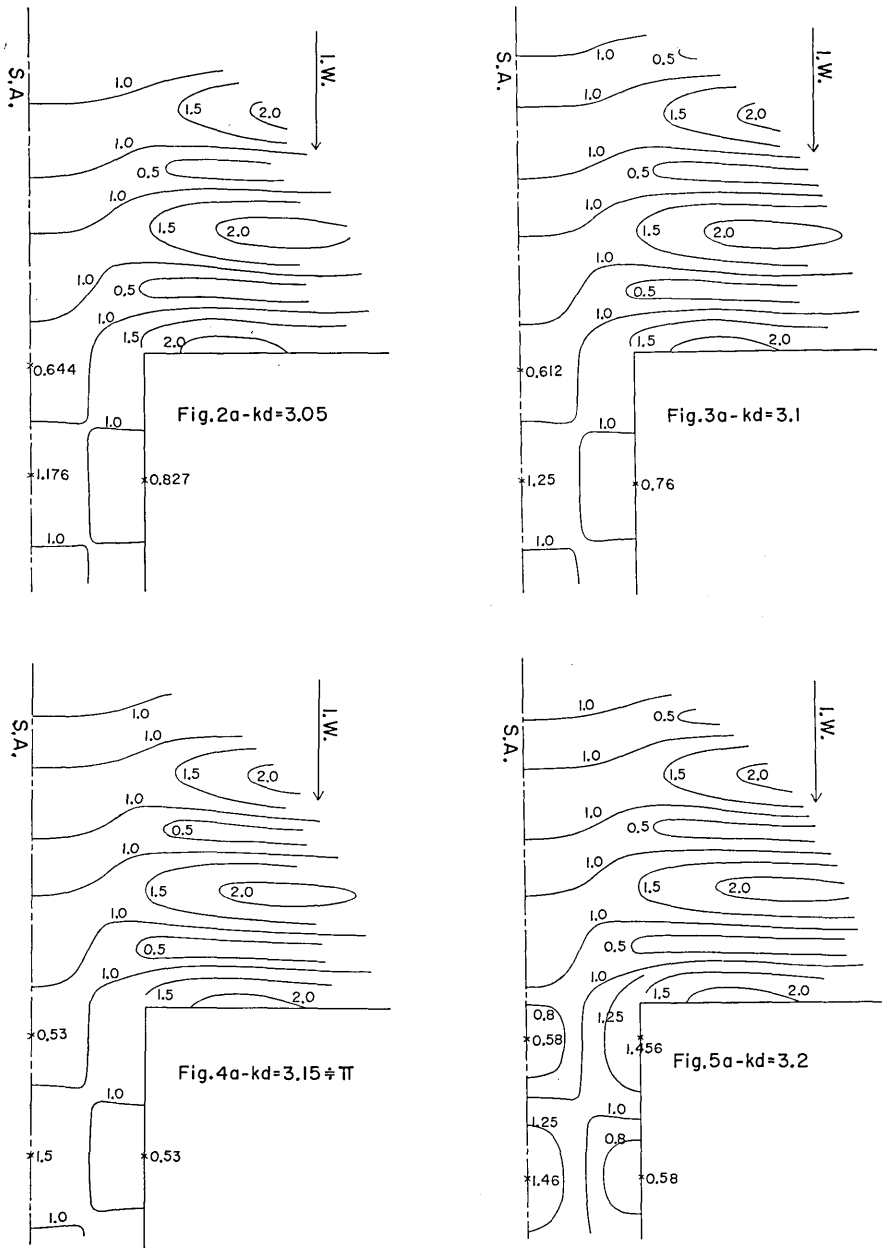

Figs. 2a-5a. Variations of the amplitude of RST wave for $kd=3.05\sim3.2$.* The above figures are based on the theory of the 15th approximation.

* **I.W.** and **S.A.** in the figures stand for "Incident Wave" and "Symmetrical Axis". This convention is followed in the subsequent figures.

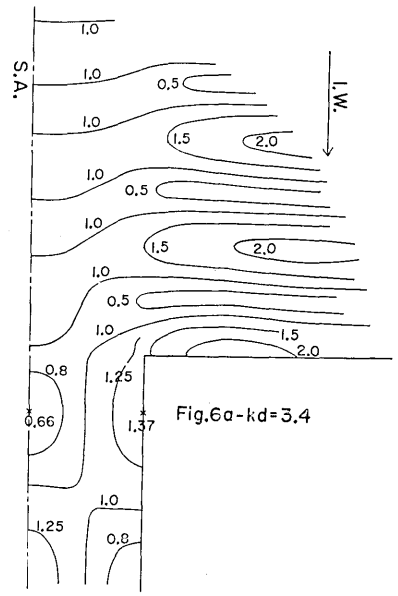

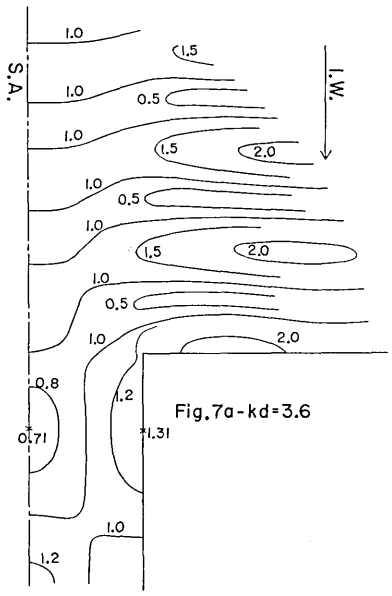

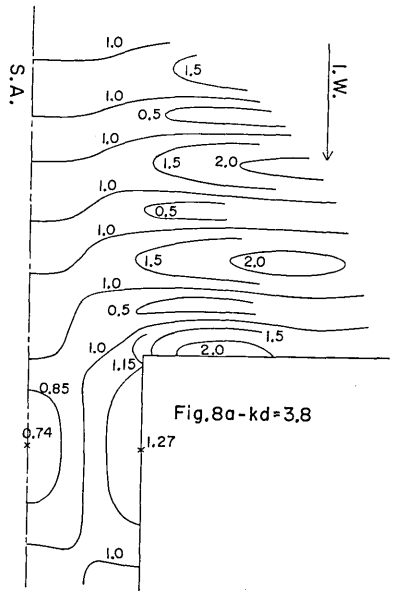

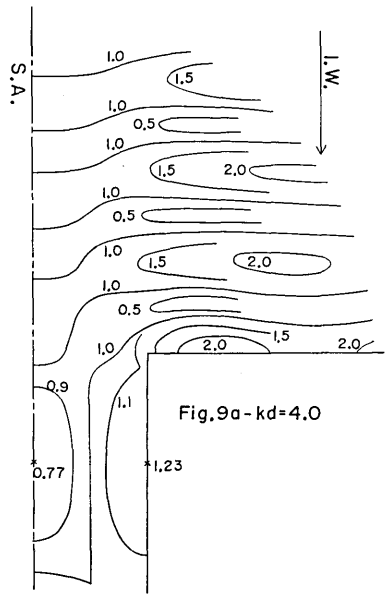

Figs. 6a-9a. Variations of the amplitude of RST wave for $kd=3.4\sim4.0$.* Fig. 6a is based on the theory of the 15th approximation and Figs. 7a-9a are that of the 17th approximation.

* See the footnote of Figs. 2a-5a.

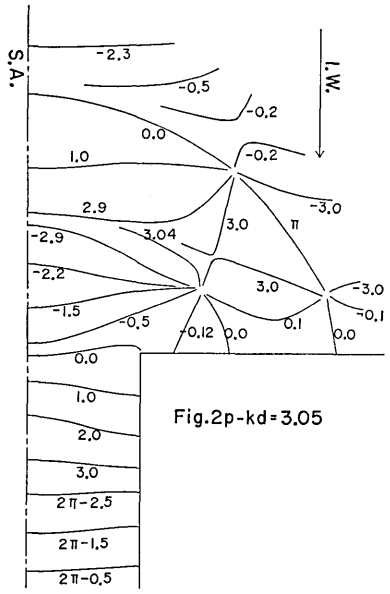

Fig.2p-kd=3.05

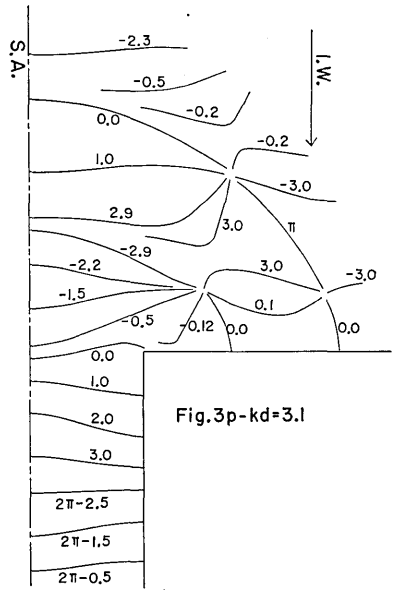

Fig.3p-kd=3.1

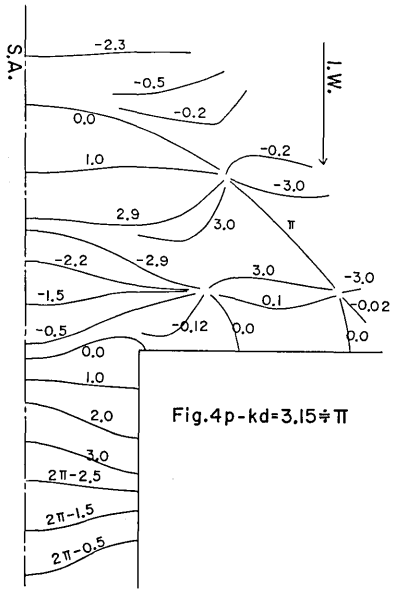

Fig.4p-kd=3.15≒π

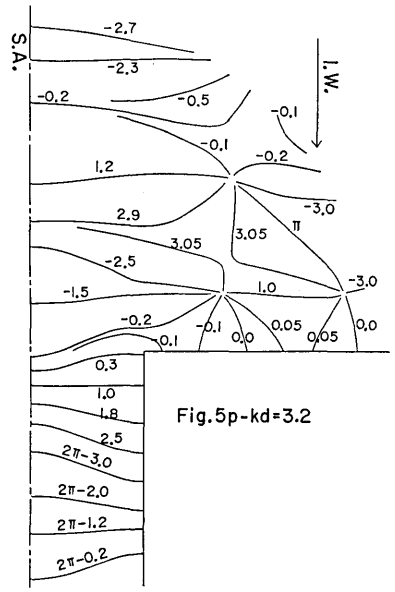

Fig.5p-kd=3.2

Figs. 2p-5p. Variations of the phase of RST wave for kd=3.05~3.2.* The figures are based on the theory of the 15th approximation.

* See the footnote of Figs. 2a-5a.

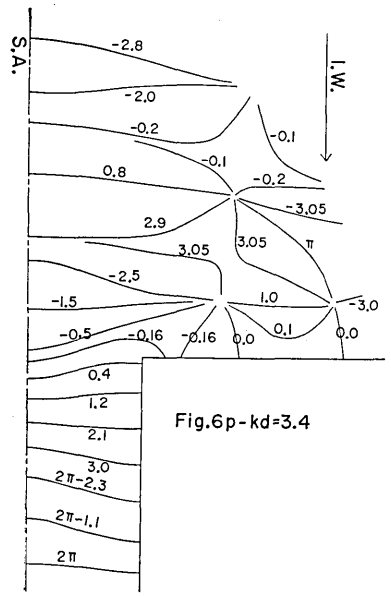

Fig.6p-kd=3.4

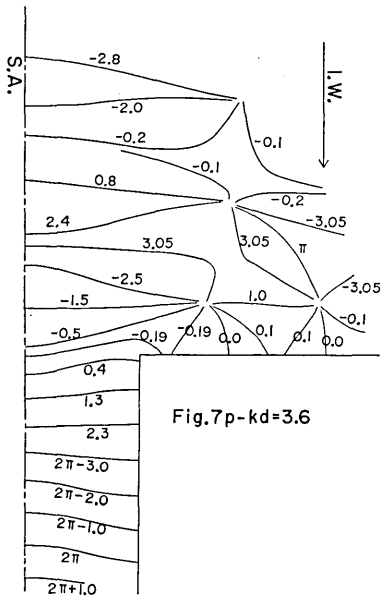

Fig.7p-kd=3.6

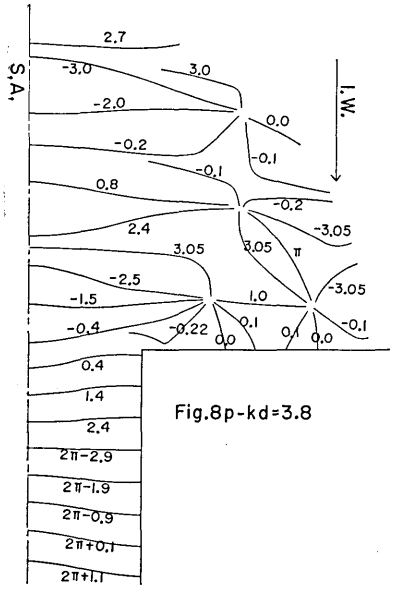

Fig.8p-kd=3.8

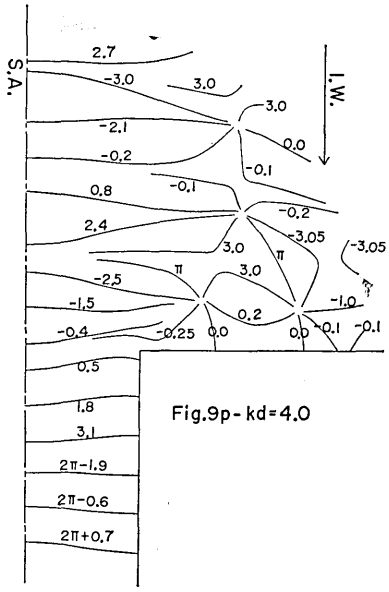

Fig.9p-kd=4.0

Figs. 6p-9p. Variations of the phase of RST wave for kd=3.4~4.0.* Fig. 6p is based on the theory of the 15th approximation and Figs. 7p-9p are that of the 17th approximation.

* See the footnote of Figs. 2a-5a.

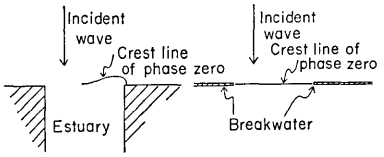

Fig. 10. Difference of the crest lines of phase zero around the estuary and breakwater.

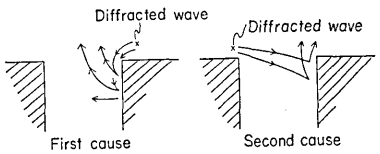

Fig. 11. Mechanism of the retardation of the phase near the corner of the estuary.

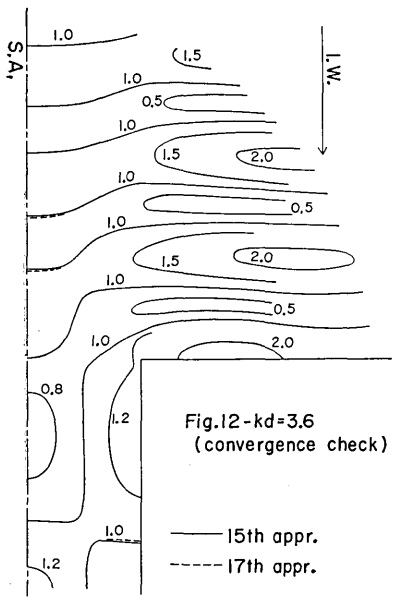

Fig. 12. Convergence check of the employed approximation.

of the above theory and the rigorous theory developed up to the present (based on the method of the buffer domain) is examined for $kd=0.5$ to 4.0, the results of which are shown in Figs. 13a to 19a for the amplitude and Figs. 13p to 19p for the phase. Some of them have already been given in Section 7 of the fifth report (*Momoi*, 1968b).

Passing through Figs. 13a(p) to 19a(p), it is found that the variations of two theories *in the open sea* are in comparatively good agreement for $kd=4.0$ as compared with the figures for the other kd. As kd decreases from 4.0 (Figs. 19a(p)) down to 3.15 (Figs. 16a(p)), the departure of two theories in the open sea continues growing to take the greatest deviation for $kd \fallingdotseq \pi$. With further decrease of kd, the above departure becomes, once again, rather smaller—the state of comparatively better agreement—, the figures of which are given by Figs. 14a(p) and 15a(p). When kd arrived at the value 0.5 (Fig. 13a(p)), the variation based on the method of mirror image deviates again from that of the rigorous theory. The first departure (for the case of $kd \fallingdotseq \pi$) is interpreted to be due to the resonance of the first mode of the wave in the canal which influences the variation in the open sea as the reflected wave, while the second departure (for the case of small kd, say $kd=0.5$) is the result of the coupling effect of two corners of the estuary. The feature is illustrated in Fig. 20.

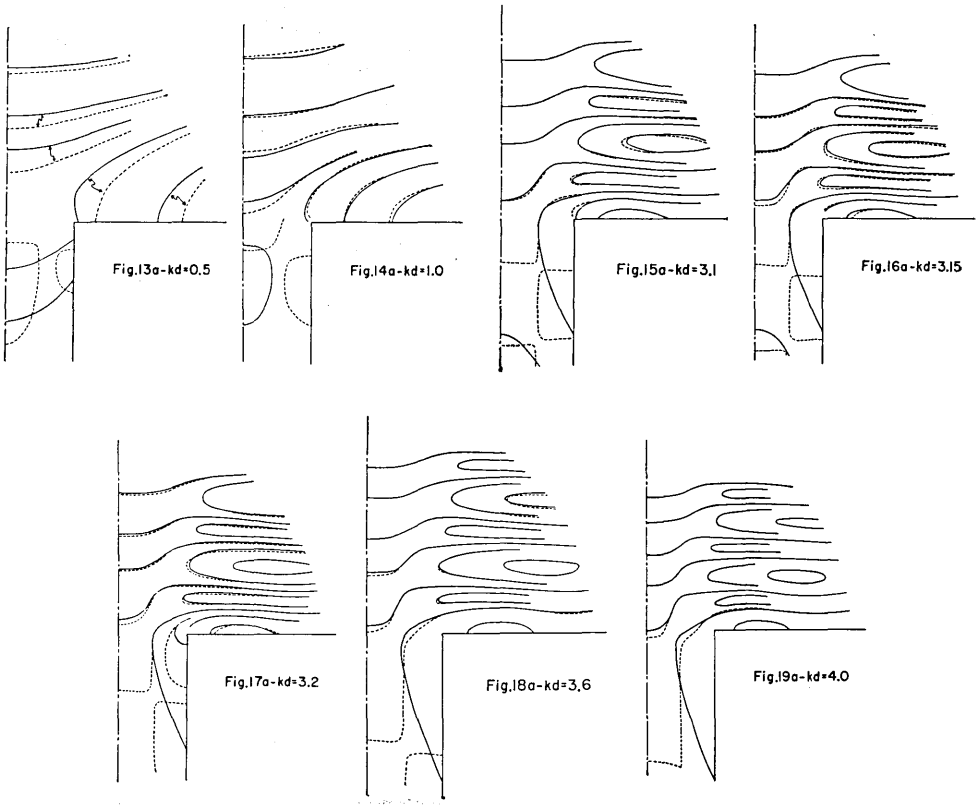

Figs. 13a–19a. Comparison of the amplitude variation based on the method of the buffer domain (rigorous method) with that by the method of mirror image for $kd=0.5\sim4.0$. The broken line stands for the former and the solid line the latter. This convention is followed in the subsequent figures concerning the phase variation.

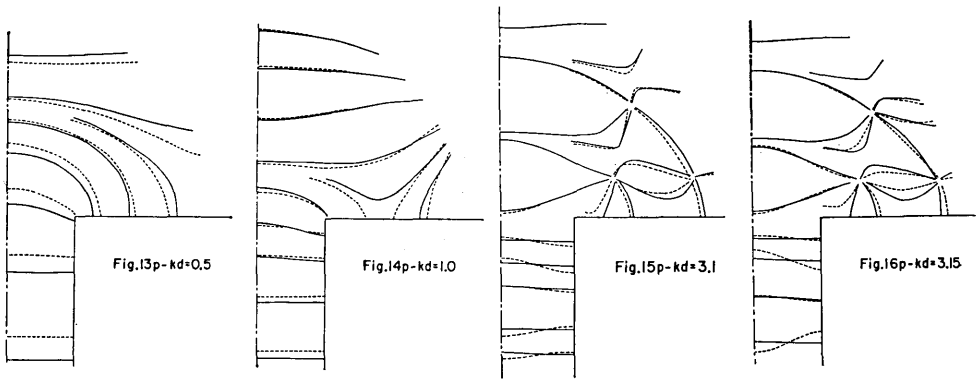

Figs. 13p–16p. Comparison of the phase variation based on the method of the buffer domain with that by the method of mirror image for $kd=0.5\sim3.15$.

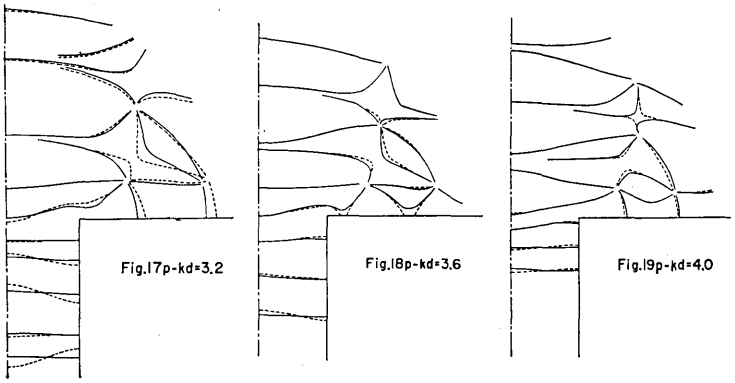

Figs. 17p-19p. Comparison of the phase variation based on the method of the buffer domain with that by the method of mirror image for $kd=3.2\sim4.0$.

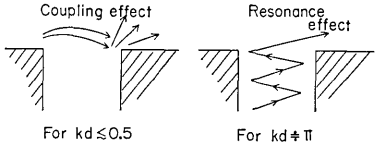

Fig. 20. Difference of the waves reflected to the open sea for $kd<0.5$ and $kd\fallingdotseq\pi$.

4. RD Wave

The further calculation of the RD (reflected and diffracted) wave is made for kd in the range of 3.05 to 4.0, following the procedure mentioned in Section 5 of the fourth paper (*Momoi*, 1968a). The computed results are given in Figs. 21a to 28a for the amplitude and Figs. 21p to 28p for the phase. In Figs. 21a to 28a, the shaded part denotes the region in which the amplitude is below 0.2 (the amplitude of the incident wave is assumed as 1.0). Passing through Figs. 21a to 28a, the above shaded region runs, in general, along the axis of the canal, particularly in the narrowest band for $kd=3.15\fallingdotseq\pi$ (the case of Fig. 23a), which refers to the resonance mode (lateral mode) of the canal. The amplitude in the canal then amounts to the value about 0.5 (a maximum value). The shaded region extends to the open sea from the canal to denote that the standing wave has not a little influence upon the open sea near the estuary. As far as the variation of the phase is concerned, it is found that the rotating wave in the canal, which has been already detected for $kd>2.2$ in the fifth work (*Momoi*, 1968b), is in a disappearing tendency with the increase of kd after taking the most conspicuous feature of the rotation for the value of $kd\fallingdotseq\pi$ (Fig. 23p). From the

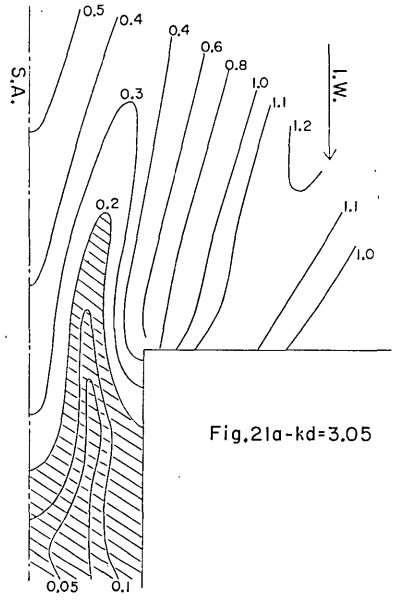

Fig.21a-kd=3.05

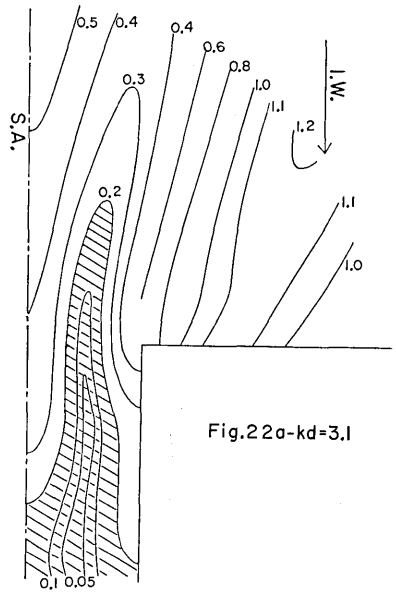

Fig.22a-kd=3.1

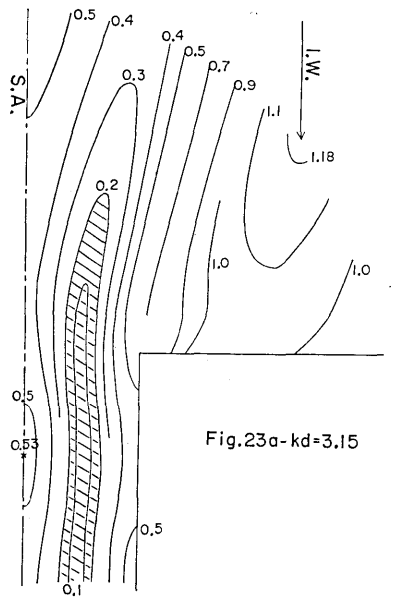

Fig.23a-kd=3.15

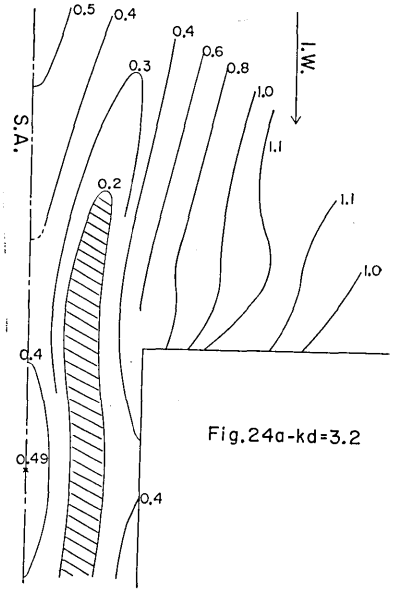

Fig.24a-kd=3.2

Figs. 21a-24a. Variations of the amplitude of RD wave $kd=3.05\sim3.2$.* The above figures are based on the theory of the 15th approximation.

* See the footnote of Figs. 2a-5a.

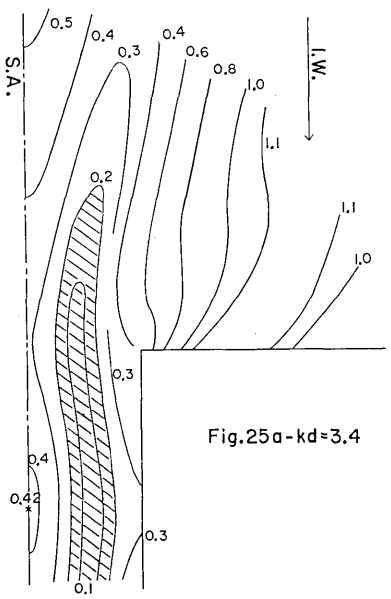

Fig.25a-kd=3.4

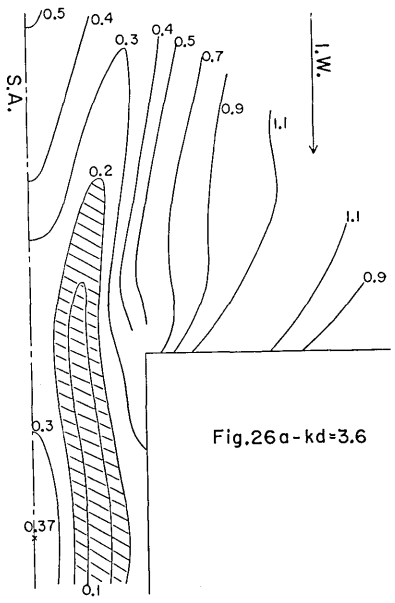

Fig.26a-kd=3.6

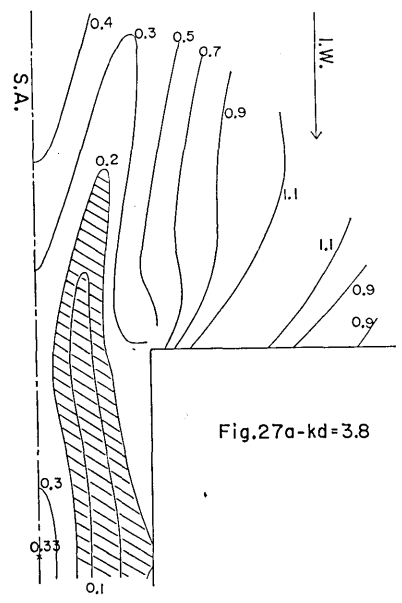

Fig.27a-kd=3.8

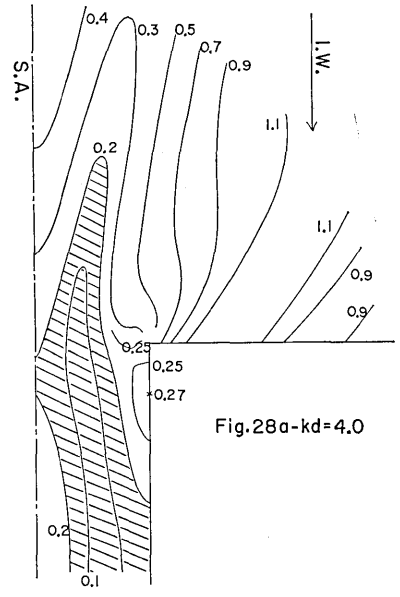

Fig.28a-kd=4.0

Figs. 25a-28a. Variations of the amplitude of RD wave for kd=3.4~4.0.* Fig. 25a is based on the theory of the 15th approximation, Figs. 26a-28a being that of the 17th approximation.

* See the footnote of Figs. 2a-5a.

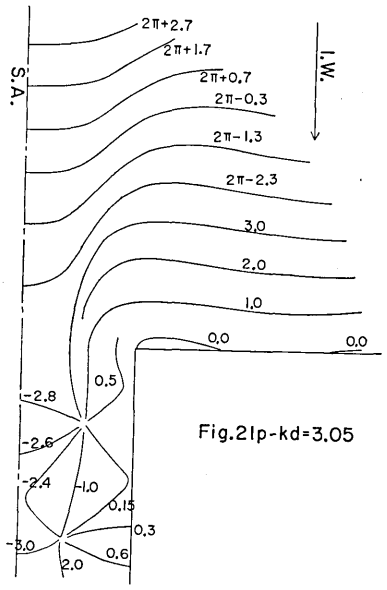

Fig.21p-kd=3.05

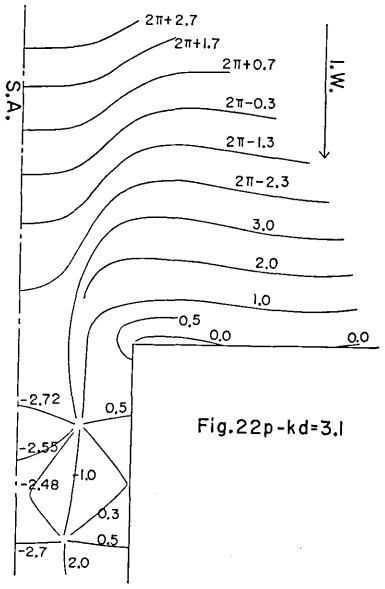

Fig.22p-kd=3.1

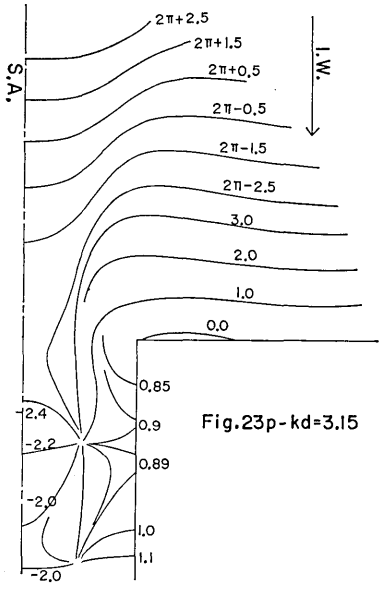

Fig.23p-kd=3.15

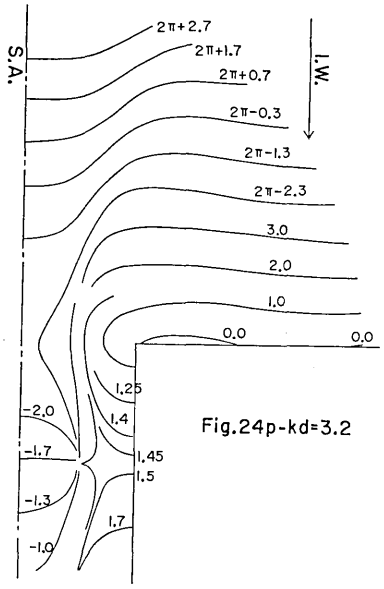

Fig.24p-kd=3.2

Figs. 21p-24p. Variations of the phase of RD wave for kd=3.05~3.2.* The above figures are based on the theory of the 15th approximation.

* See the footnote of Figs. 2a-5a.

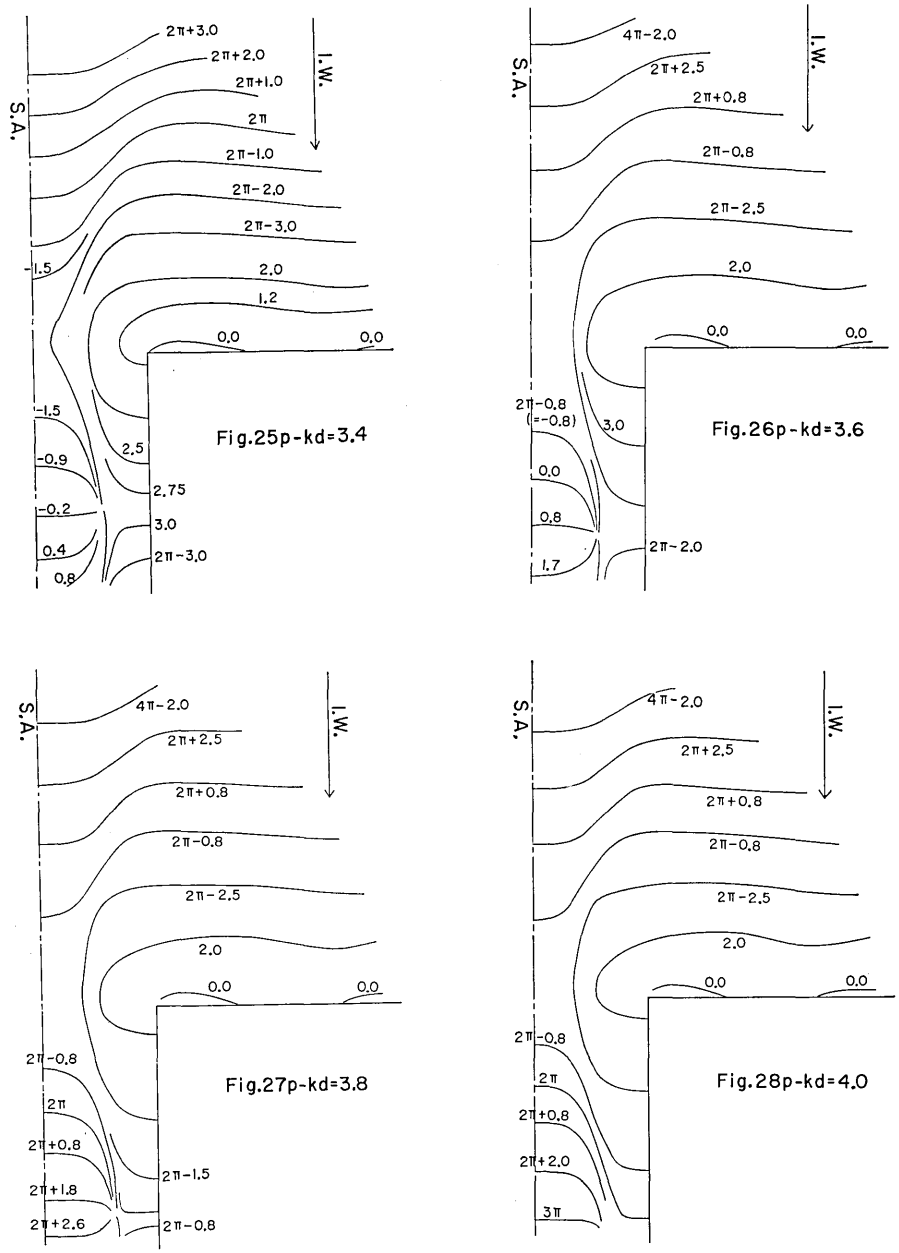

Figs. 25p-28p. Variations of the phase of RD wave for kd=3.4~4.0.* Fig. 25p is based on the theory of the 15th approximation, Figs. 26p-28p being that of the 17th approximation.

* See the footnote of Figs. 2a-5a.

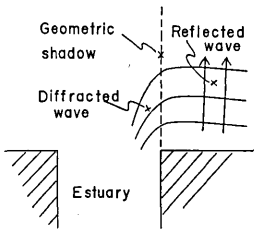

Fig. 29a. Generation of geometric shadow of RD wave for kd over 3.0.

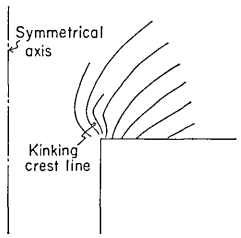

Fig. 29b. Kinking crest line of RD wave near the corner of the estuary. The figure is depicted for $kd=0.5$.

above fact, the rotating wave is considered to be produced by the resonating wave in the canal. Comparing these figures with the figures of the phase of RD wave in the previous works (Figs.2b–13b and 17b–24b of the fourth and fifth papers (*Momoi*, 1968a and 1968b)), the diffracted wave toward the mouth of the estuary is definitely separated, for kd over about 3.0, from the reflected wave from the coast to the outer sea with clear geometric shadow (see Fig. 29a).

In the fourth paper (*Momoi*, 1968a), we have discussed an appearance of the kinking crest line in the nearby waters of the corner of the estuary for the RD wave of comparatively long wave-length. We have then used the approximated power series for the Bessel function $J_m(z)$ in the calculation of the integrals

$$\left.\begin{aligned} I(J_{2n},\ m)&=\int_0^{kd} J_{2n}(z)\cos\frac{m\pi}{kd}zdz \\ \text{and}\quad I\left(\frac{J_{2n+1}}{r},\ m\right)&=(2n+1)\int_0^{kd}\frac{J_{2n+1}(z)}{z}\cos\frac{m\pi}{kd}zdz\,, \end{aligned}\right\}$$

which are described in (5) of the fourth paper (*Momoi*, 1968a). In order to avoid the misunderstanding that the above-mentioned kinking crest line might be the result of the use of the approximated power series of the Bessel function, the existence of the kink is ascertained through the direct integration of the above integrals with the use of the rigorous Bessel function. The method of the integration is Filon's method described in Section 2 of the fifth work (*Momoi*, 1968b). The calculated phase variation is that for $kd=0.5$, which is shown in Fig. 29b. According to the figure, the kinking crest line is definitely found in the waters near the corner of the estuary.

5. Secondary Reflection (SR Wave)

SR wave is an abbreviation of the secondarily reflected wave except the primary reflection from RST wave, which is estimated by

the following procedure. In the fifth work (*Momoi*, 1968b), we have developed the approximated theory by the method of mirror image (refer to Section 7 of the above work). Only the primary reflection is then allowed for. The subtraction of the above approximated solution (based on the method of mirror image) from the rigorous solution (based on the method of the buffer domain) developed so far makes possible the estimation of the secondary reflection around the estuary. Let ζ_{rig} and ζ_{mir} be, respectively, the wave heights given by (13) to (15) of the fifth paper (*Momoi*, 1968b) and (22) of the same paper. The secondary reflection ζ_{sr} of the wave is then expressed, approximately, by

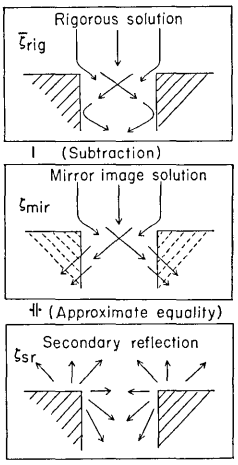

Fig. 30. Schema of equation (1).

$$\zeta_{sr} \fallingdotseq \bar{\zeta}_{rig} - \zeta_{mir} \tag{1}$$

($\bar{\zeta}_{rig}$ is the conjugate value of ζ_{rig}, which refers to the conversion of the incident wave from $\exp(-i\omega t - iky)$ to $\exp(+i\omega t + iky)$), which is illustrated in Fig. 30. The results of the calculation are given in Figs. 31a to 42a for the amplitude and Figs. 31p to 42p for the phase. The numerals stated in the figures are respectively $|\zeta_{sr}|$ and $\arg \zeta_{sr}$ for the amplitude and phase.

In the figures of the amplitude for $kd=0.5$ to 1.4 (Figs. 31a to 36a), the region of high amplitude is found along the coast facing the open sea. According to Figs. 31p to 36p, the above high amplitude area is characterized by the emitting behavior of the reflected wave (refer to Fig. 43) which is the secondary reflection of the diffracted wave from the other coast of the estuary instead of the reflection of the directly diverted and reflected wave shown in Fig. 20 of the third work (*Momoi*, 1966).

In the previous paper (*Momoi*, 1966), we have discussed an appearance of the crest line in triangular form for the wave of large wave-length near the estuary. As exposed in the above, the secondary reflected wave is produced along the coast facing the open sea. The above secondary wave is considered one of the causes for the generation of the triangular crest line. For the form of the crest line, the reader should refer to Fig. 9 of the previous paper (*Momoi*, 1966).

Through the figures relevant to the amplitude, the area over 0.1 (the amplitude of the incident wave is assumed as 1.0) is shadowed.

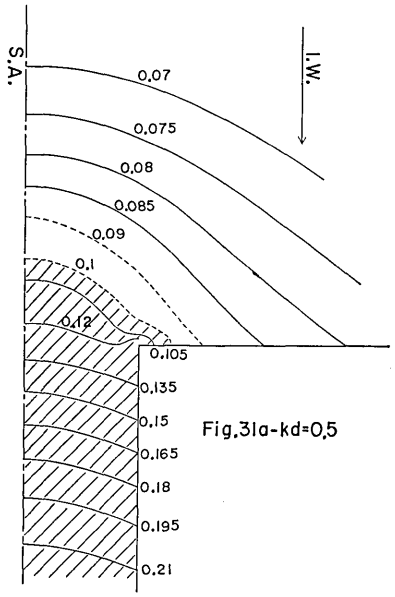

Fig. 31a. Variation of the amplitude of SR wave for $kd=0.5$* (based on the theory of the 9th approximation).

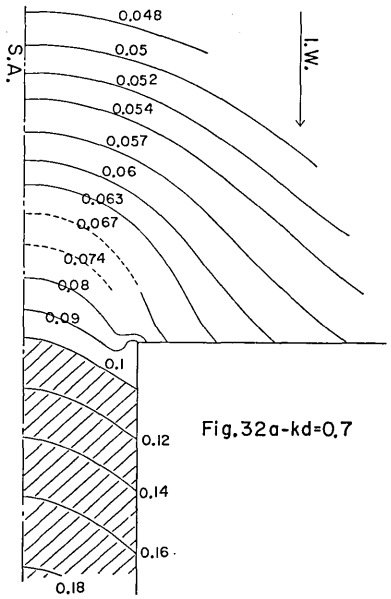

Fig. 32a. Variation of the amplitude of SR wave for $kd=0.7$* (based on the theory of the 11th approximation).

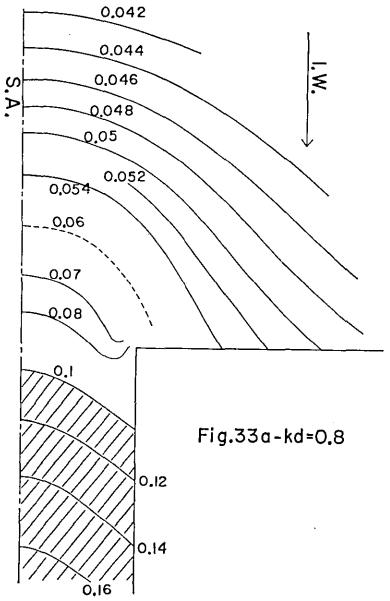

Fig. 33a. Variation of the amplitude of SR wave for $kd=0.8$* (based on the theory of the 11th approximation).

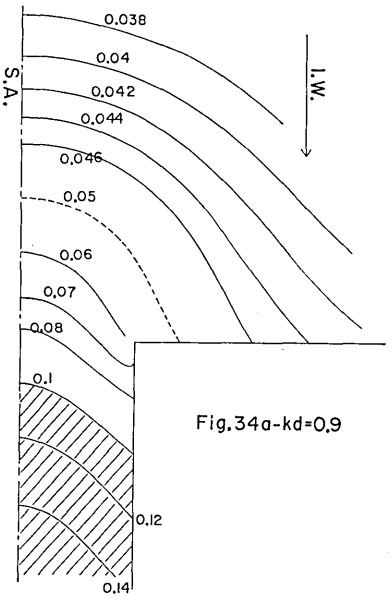

Fig. 34a. Variation of the amplitude of SR wave for $kd=0.9$* (based on the theory of the 11th approximation).

* See the footnote of Figs. 2a-5a.

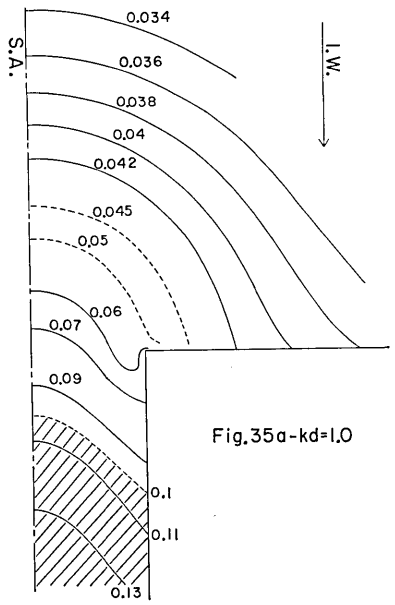

Fig. 35a. Variation of the amplitude of SR wave for $kd=1.0$* (based on the theory of the 11th approximation).

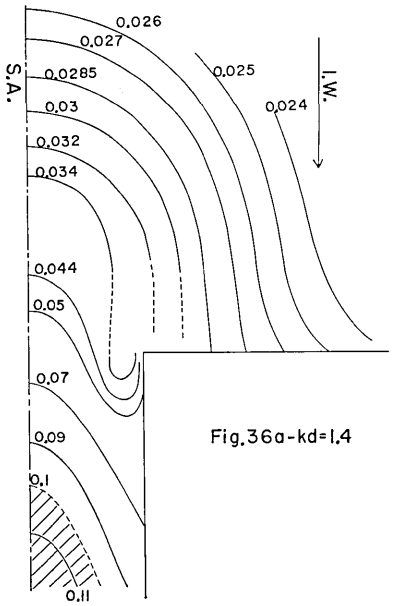

Fig. 36a. Variation of the amplitude of SR wave for $kd=1.4$* (based on the theory of the 13th approximation).

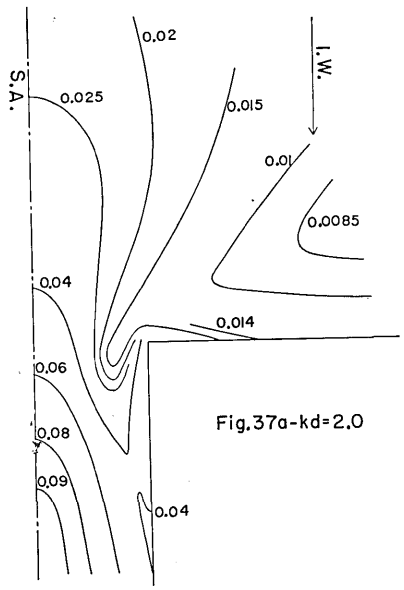

Fig. 37a. Variation of the amplitude of SR wave for $kd=2.0$* (based on the theory of the 15th approximation).

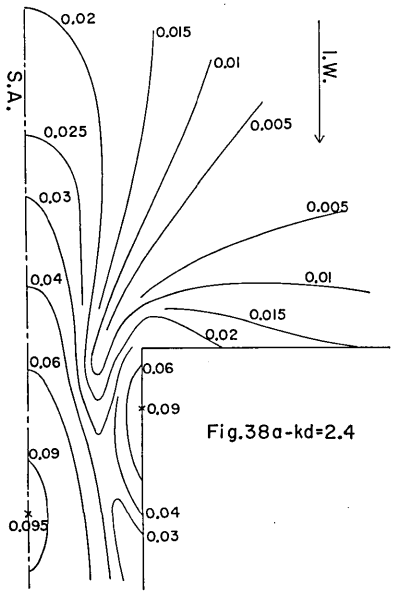

Fig. 38a. Variation of the amplitude of SR wave for $kd=2.4$* (based on the theory of the 15th approximation).

* See the footnote of Figs. 2a-5a.

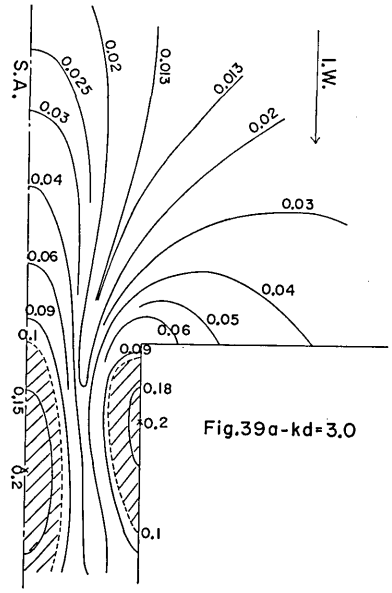

Fig. 39a. Variation of the amplitude of SR wave for $kd=3.0$* (based on the theory of the 17th approximation).

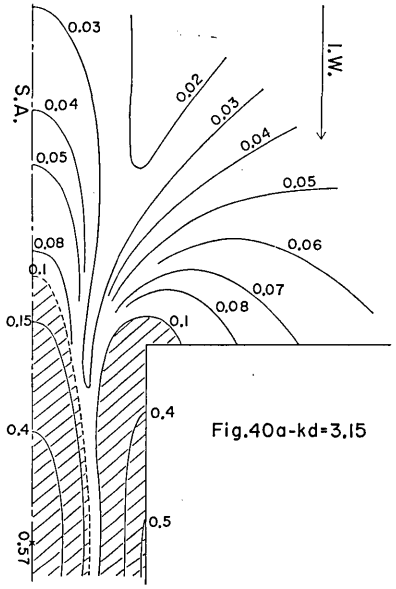

Fig. 40a. Variation of the amplitude of SR wave for $kd=3.15$* (based on the theory of the 17th approximation).

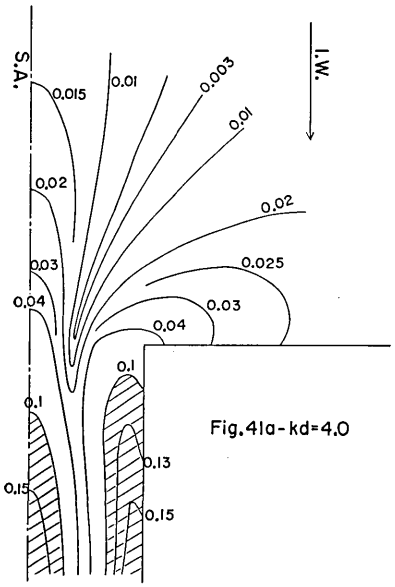

Fig. 41a. Variation of the amplitude of SR wave for $kd=4.0$* (based on the theory of the 19th approximation).

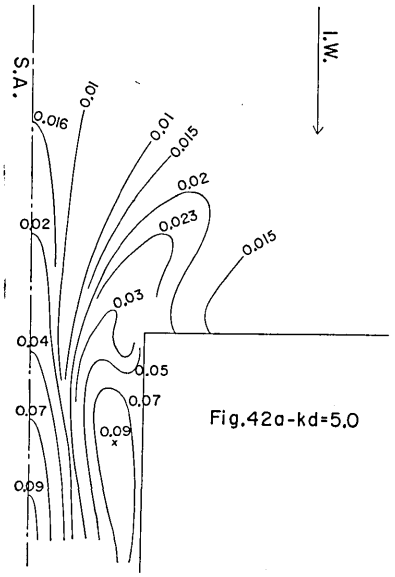

Fig. 42a. Variation of the amplitude of SR wave for $kd=5.0$* (based on the theory of the 21st approximation).

* See the footnote of Figs. 2a-5a.

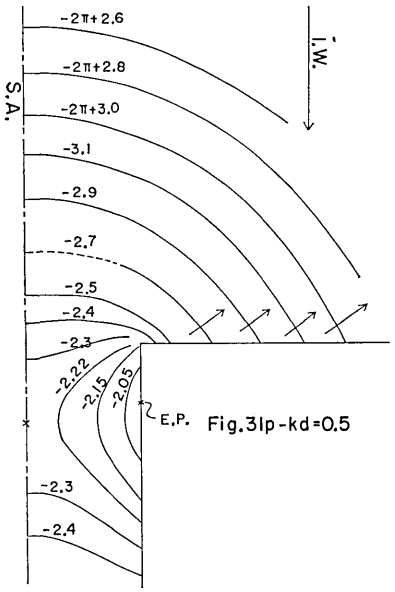

Fig. 31p. Variation of the phase of SR wave for $kd=0.5$** (based on the theory of the 9th approximation).

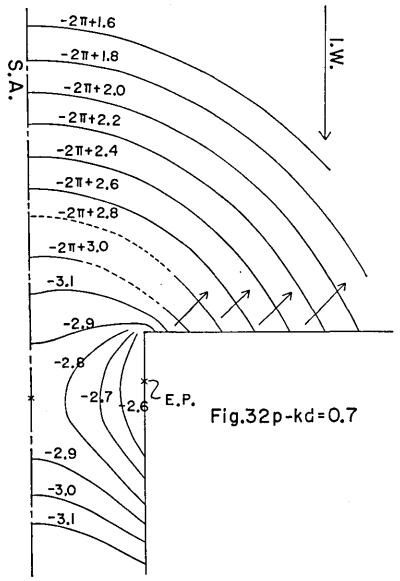

Fig. 32p. Variation of the phase of SR wave for $kd=0.7$** (based on the theory of the 11th approximation).

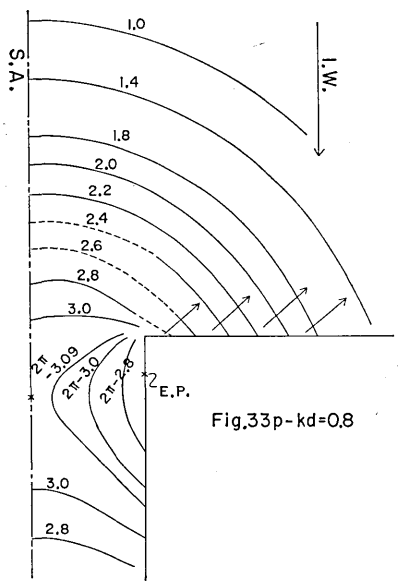

Fig. 33p. Variation of the phase of SR wave for $kd=0.8$** (based on the theory of the 11th approximation).

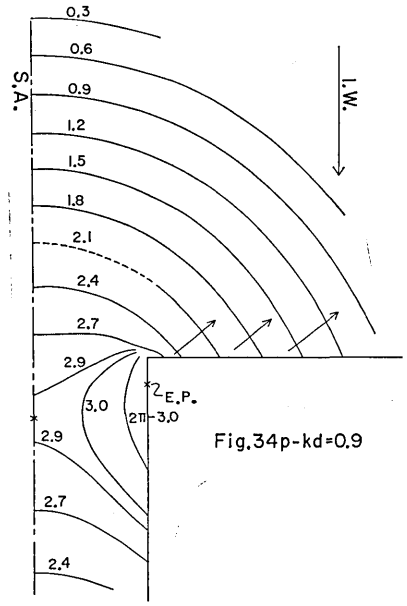

Fig. 34p. Variation of the phase of SR wave for $kd=0.9$** (based on the theory of the 11th approximation).

** For **I.W.** and **S.A.** stated in the figures, the reader should refer to the footnote of Figs. 2a-5a. **E.P.** in the figures denotes "Emitting Point" of the wave.

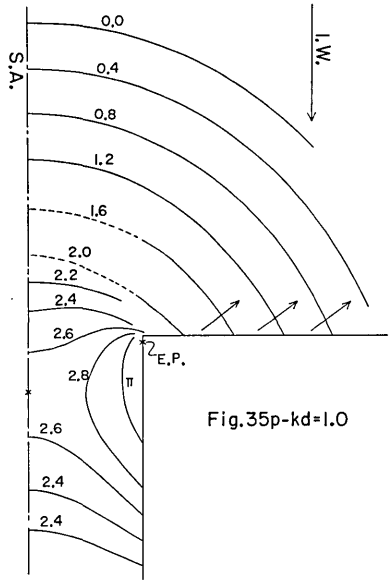

Fig. 35p. Variation of the phase of SR wave for $kd=1.0$** (based on the theory of the 11th approximation).

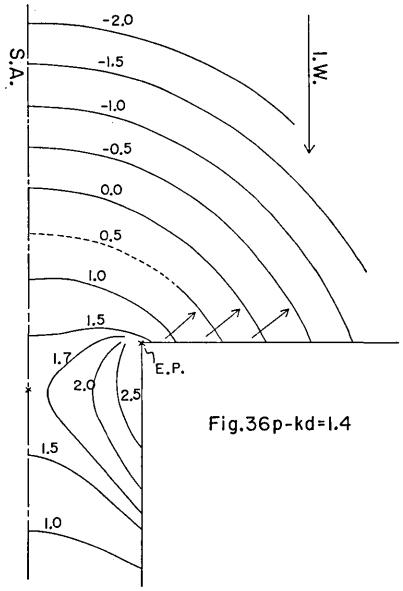

Fig. 36p. Variation of the phase of SR wave for $kd=1.4$** (based on the theory of the 13th approximation).

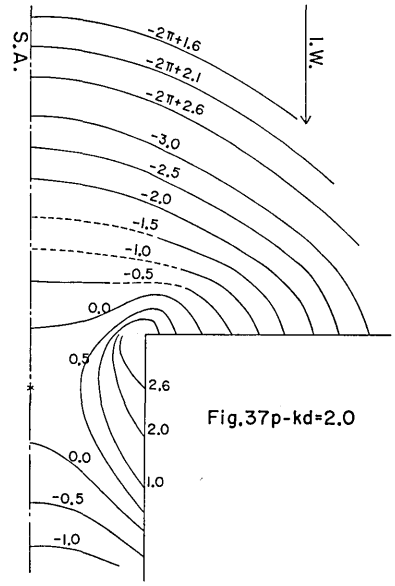

Fig. 37p. Variation of the phase of SR wave for $kd=2.0$* (based on the theory of the 15th approximation).

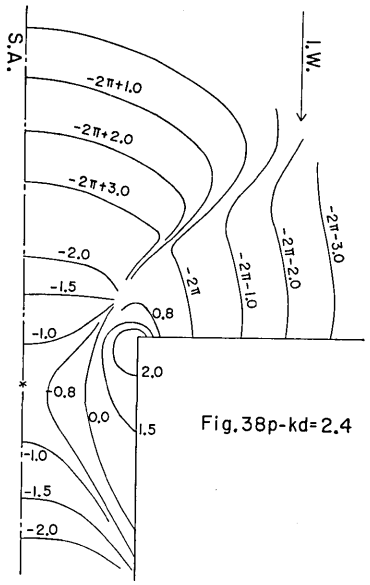

Fig. 38p. Variation of the phase of SR wave for $kd=2.4$* (based on the theory of the 15th approximation).

* See the footnote of Figs. 2a-5a.
** See the footnote of Figs. 31p-34p.

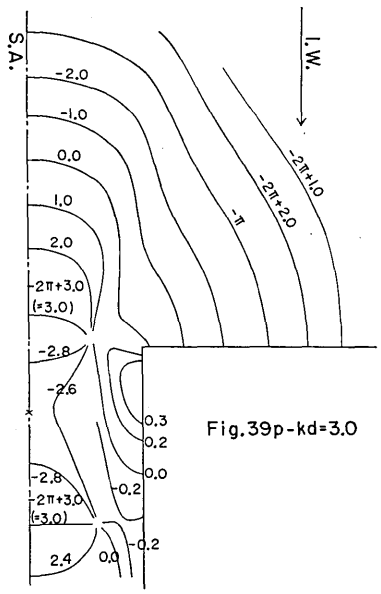

Fig. 39p. Variation of the phase of SR wave for $kd=3.0$* (based on the theory of the 17th approximation).

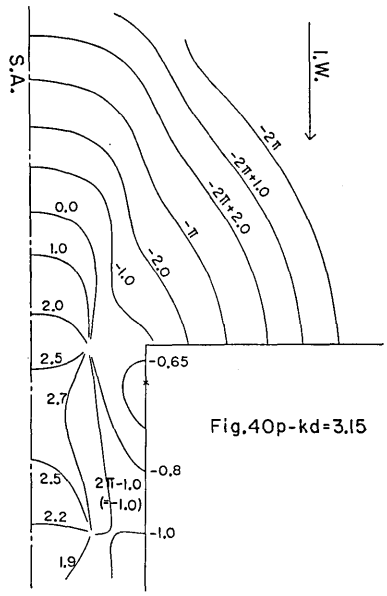

Fig. 40p. Variation of the phase of SR wave for $kd=3.15$* (based on the theory of the 17th approximation).

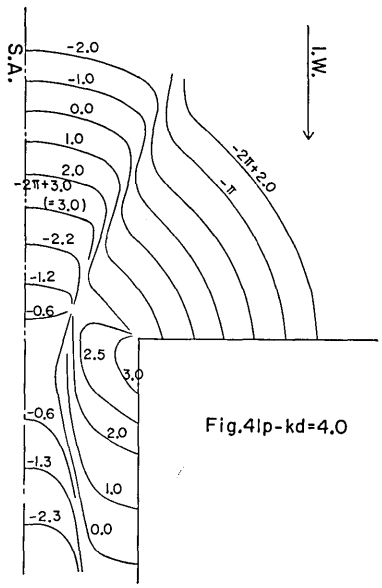

Fig. 41p. Variation of the phase of SR wave for $kd=4.0$* (based on the theory of the 19th approximation).

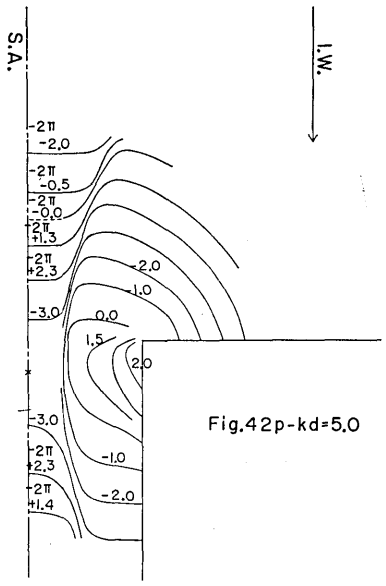

Fig. 42p. Variation of the phase of SR wave for $kd=5.0$* (based on the theory of the 21st approximation).

* See the footnote of Figs. 2a-5a.

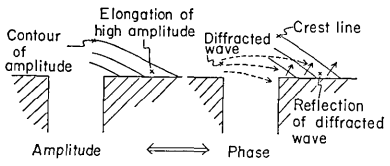

Fig. 43. Secondary reflection at the coast facing the open sea.

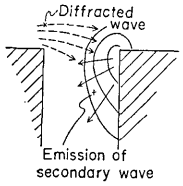

Fig. 44. Emitting mechanism of the secondary wave.

According to these figures, the secondary reflections (including at present the higher order reflections) are comparatively greater for small kd (Figs. 31a and 32a) than for large kd except the values near $kd=3.15\fallingdotseq\pi$ (Fig. 40a, i.e., the case of the resonance of the first mode in the canal). At the value $kd\fallingdotseq\pi$, the two regions of high amplitude extend along the symmetrical axis and the bank of the canal with node (low amplitude) between them to suggest the exciting of the lateral resonance (refer to Fig. 40a). The excitation amounts to about 0.5 in amplitude.

In Figs. 31p to 42p (the figures of the phase variation), the most conspicuous feature is an emission of the wave from the bank of the canal near the corner of the estuary. The mechanism is such that, referring to Fig. 44, the diffracted wave from the left corner of the estuary arrives at the right corner to produce the emission of the secondary wave along the right-hand bank of the canal. For small kd (say Figs. 31p to 34p), the point of the above emission is located at a point slightly away from the corner of the estuary in the tendency that the point approaches the corner with the increase of kd from 0.5 (Fig. 31p) to 1.0 (Fig. 35p). The cause might be attributed to the stronger diffraction of the diffracted wave toward the inside of the canal for small kd.

6. Effect of the Banks of the Canal

In order to examine, in particular, the effect of the banks for small kd, the following procedure is considered. Let ζ_{est} and ζ_{bw} be, respectively, the wave heights of the estuary (the rigorous solution) given by (13) to (15) of the fifth work (*Momoi*, 1968b) and by (21) to (23) of the paper concerning the long wave around the breakwater gap (*Momoi*, 1967b). The effect of the banks ζ_{eb} is examined by

$$\zeta_{eb}=\overline{\zeta}_{est}-\overline{\zeta}_{bw}\ , \tag{2}$$

where the quantities with the bar are the conjugate values of the relevant quantities showing the conversion of the incident wave from

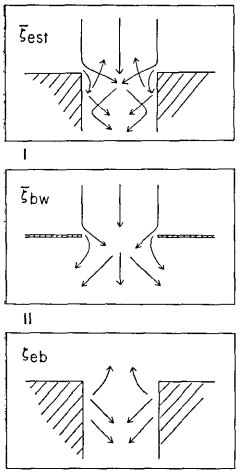

Fig. 45. Scema of equation (2).

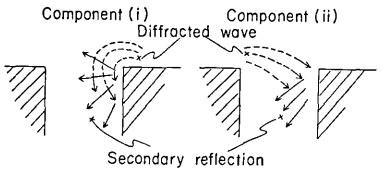

Fig. 46. Composition of the wave described in equation (2).

$\exp(-i\omega t-iky)$ to $\exp(+i\omega t+iky)$. Equation (2) is explained figuratively in Fig. 45. The difference between equations (1) and (2) is as follows. In the case of this section (equation (2)), the secondary reflection is composed of two components, that is to say (i) the reflection of the wave at the bank which is diffracted from the coast facing the open sea to the bank directly behind and (ii) that which is produced by the arrival of the wave diffracted from the other coast (see Fig. 46), while, in the case of the foregoing section (equation (1)), the secondary reflection refers to only the component (ii) described above.

Using equation (2), the calculation of ζ_{eb} is carried out, the results of which are shown in Figs. 47a to 57a for the amplitude and Figs. 47p to 57p for the phase. The values stated in the figures are $|\zeta_{eb}|$ for the amplitude and $\arg\zeta_{eb}$ for the phase.

In Figs. 47a to 57a, the region over the value 0.4 is shadowed. Comparing the above figures with those of the amplitude variation of the secondary reflection (Section 5) with the same range of kd, i.e., Figs. 31a to 37a, it is found that the secondary reflected wave of the type (i) described above weighs down that of the type (ii) in such a way that the intensity of the former is about four or five times that of the latter.

In the figures of the phase variation (Figs. 47p to 57p), the emitting point of the wave is the very point of the corner of the estuary other than that of SR wave in the previous section. As will be shown in Section 8 (Reflection of the Diffracted Wave around the Right-angled Corner), the secondary wave reflected from the leeward coast of the right-angled corner leaves from the very point of the corner. Accordingly, the above behavior of the emitting point in the estuary is interpreted to come from the overwhelming of the secondary wave of the type (i).

Comparing Figs. 47p to 52p with Figs. 31p to 35p, the obliquely emitted wave along the coast such as exposed in the figures of the

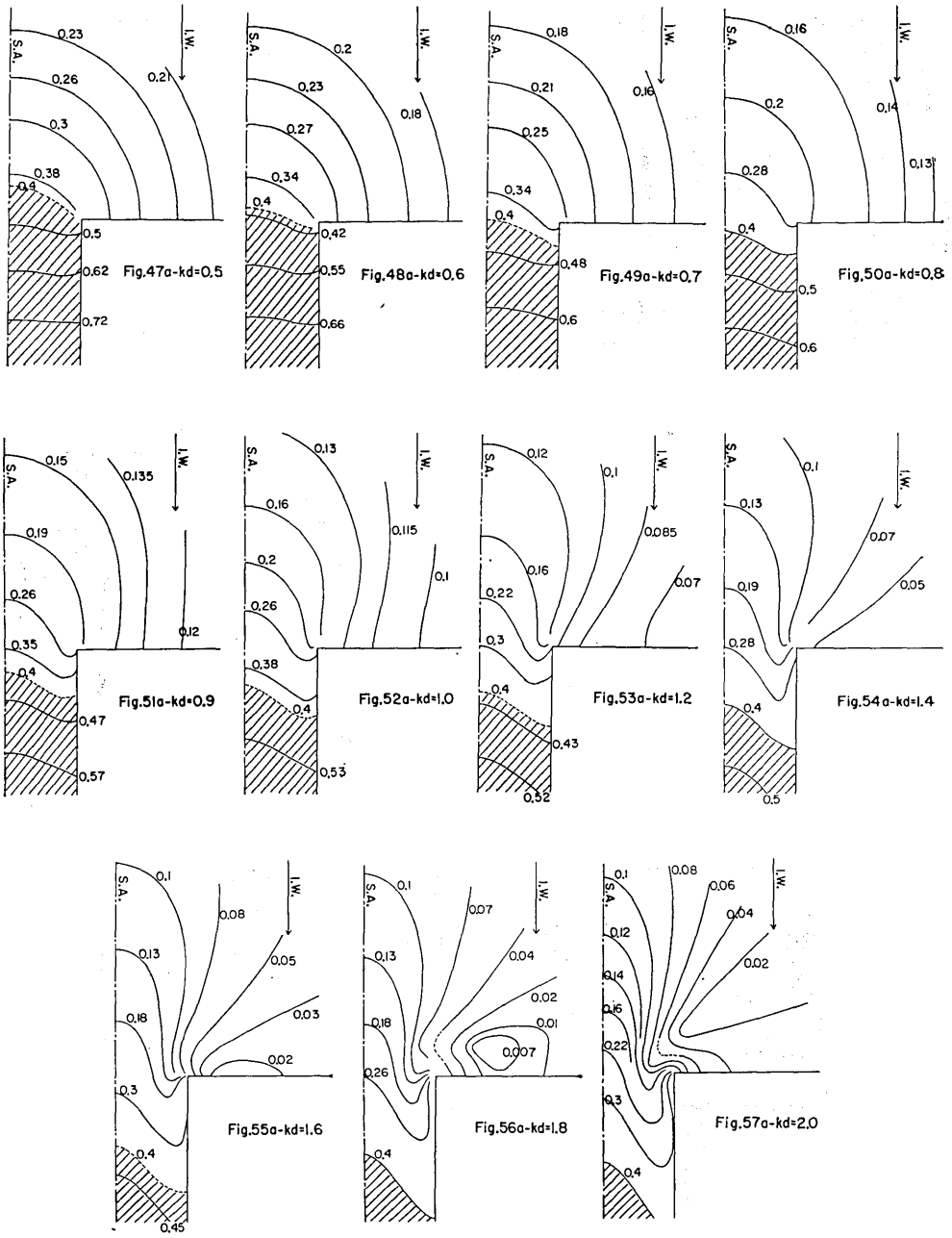

Figs. 47a-57a. Variations of the intensity $|\zeta_{eb}|$ denoting the effect of the banks of the canal of the estuary for kd=0.5 to 2.0.*

* See the footnote of Figs. 2a-5a.

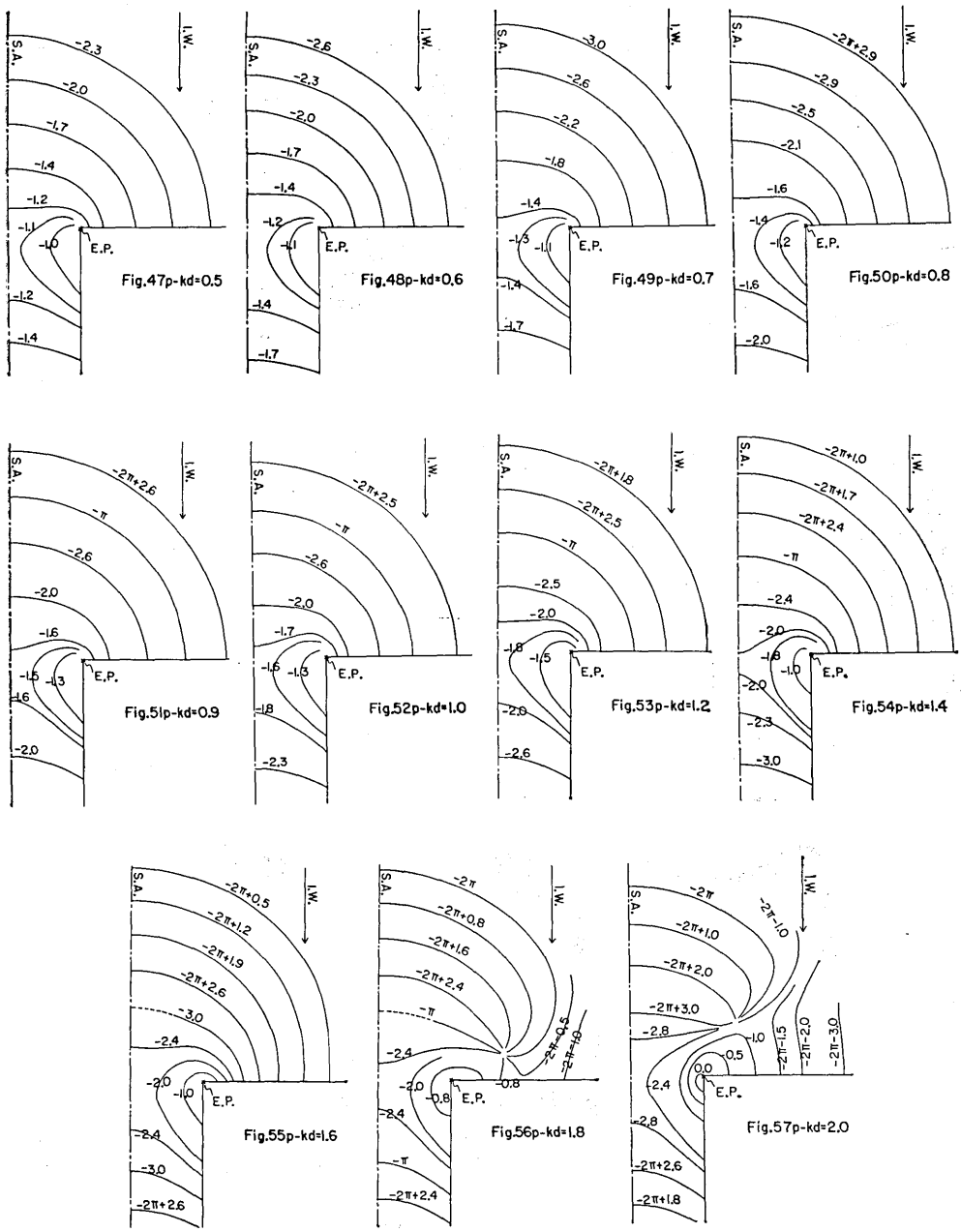

Figs. 47p–57p. Variations of the phase arg ζ_{eb} denoting the effect of the the banks of canal of the estuary for $kd=0.5$ to 2.0.**

** See the footnote of Figs. 31p to 34p.

latter is not found in the former, but the wave advances along the coast. This fact denotes that the obliquely emitted wave along the coast found in Section 5 is definitely based on the secondary reflection of the diffracted wave from the other coast (refer to Fig. 43).

7. Effect of the Corner upon the Diffracted Wave from the Other Corner

In this section, the effect of the corner of the estuary upon the wave which is diffracted from the other corner is examined. The method of the examination is as follows. Let ζ_{est} and ζ_{rc} be, respectively, the wave height given by (13) to (15) of the fifth work concerning the estuary (*Momoi*, 1968b) and the wave height around the right-angled corner given by (17) of the above paper. The geometry of the model of the right-angled corner is then the same as that of the right-hand corner of the estuary with the transfer of the origin of the coordinate of the former to the midpoint of the mouth of the estuary. The estimation of the effect of the right-hand corner ζ_{ec} of the estuary upon the diffracted wave from the left-hand corner is made by the subtraction ζ_{rc} from $\overline{\zeta}_{est}$ (the conjugate value of ζ_{est} which refers to the conversion of the incident wave from $\exp(-i\omega t-iky)$ to $\exp(+iky+iky)$), i.e.,

$$\zeta_{ec} \doteqdot \overline{\zeta}_{est}-\zeta_{rc} \,. \tag{3}$$

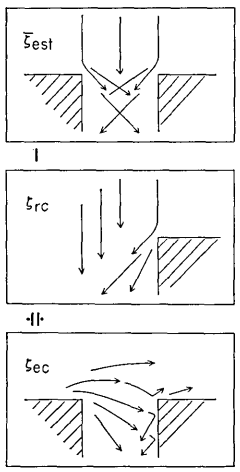

Fig. 58. Schema of equation (3).

The above equation is illustrated in Fig. 58. Though the origin of the coordinate of the model of the right-angled corner is transferred to the origin of the estuary (the midpoint of the mouth of the estuary), the solution around the single right-angled corner is still described by (17) of the fifth paper (*Momoi*, 1968b) owing to the normal incidence of the invading wave.

Using (3), the calulation of ζ_{ec} is carried out, the results of which are shown in Figs. 59a to 69a for the amplitude and Figs. 59p to 68p for the phase. The values stated in the figures denote $|\zeta_{ec}|$ for the amplitude and $\arg \zeta_{ec}$ for the phase. The waves expressed by equation (3) are not simply the waves arriving at the right corner from the left one, but include the multiply reflected waves between two corners (or banks of the canal). The former, however, might be interpreted to be, as the first approximation, overweighing upon the

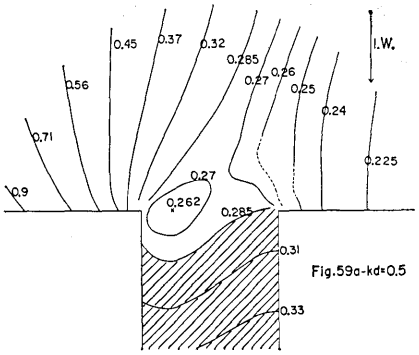

Fig. 59a. Variation of the intensity $|\zeta_{ec}|$ denoting the effect of the right corner upon the wave diffracted from the left corner for $kd=0.5$.*

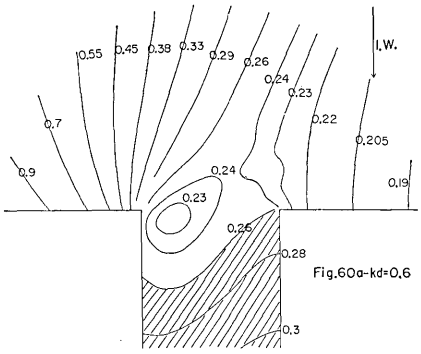

Fig. 60a. Variation of the intensity $|\zeta_{ec}|$ denoting the effect of the right corner upon the wave diffracted from the left corner for $kd=0.6$.*

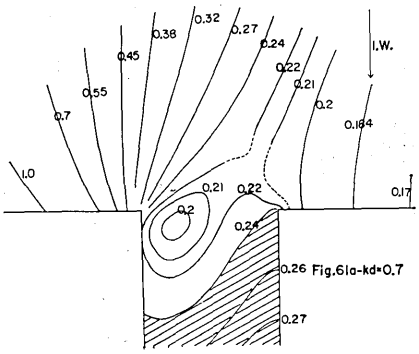

Fig. 61a. Variation of the intensity $|\zeta_{ec}|$ denoting the effect of the right corner upon the wave diffracted from the left corner for $kd=0.7$.*

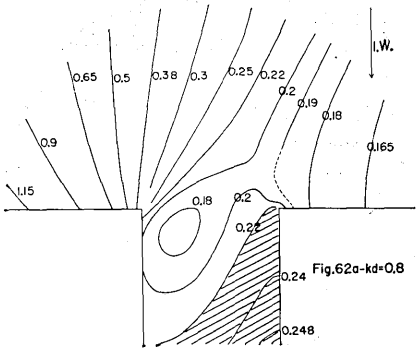

Fig. 62a. Variation of the intensity $|\zeta_{ec}|$ denoting the effect of the right corner upon the wave diffracted from the left corner for $kd=0.8$.*

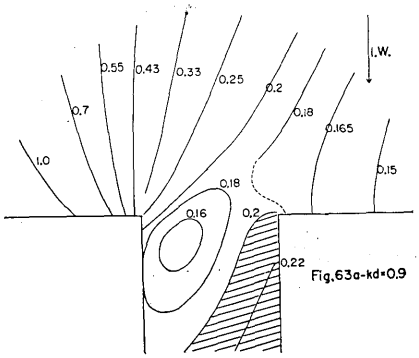

Fig. 63a. Variation of the intensity $|\zeta_{ec}|$ denoting the effect of the right corner upon the wave diffracted from the left corner for $kd=0.9$.*

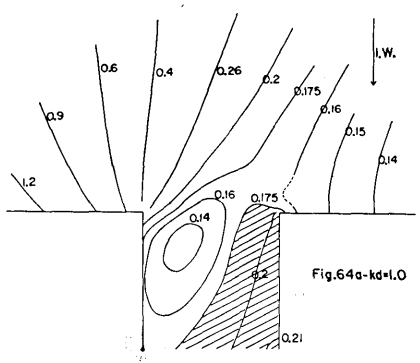

Fig. 64a. Variation of the intensity $|\zeta_{ec}|$ denoting the effect of the right corner upon the wave diffracted from the left corner for $kd=1.0$.*

* See the footnote of Figs. 2a-5a.

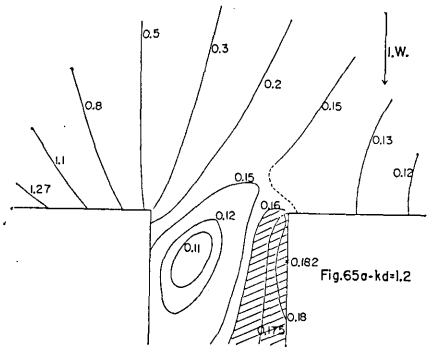

Fig. 65a. Variation of the intensity $|\zeta_{ec}|$ denoting the effect of the right corner upon the wave diffracted from the left corner for $kd=1.2$.*

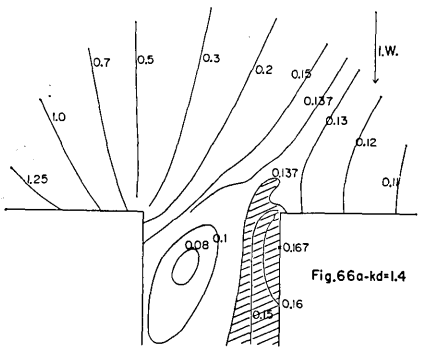

Fig. 66a. Variation of the intensity $|\zeta_{ec}|$ denoting the effect of the right corner upon the wave diffracted from the left corner for $kd=1.4$.*

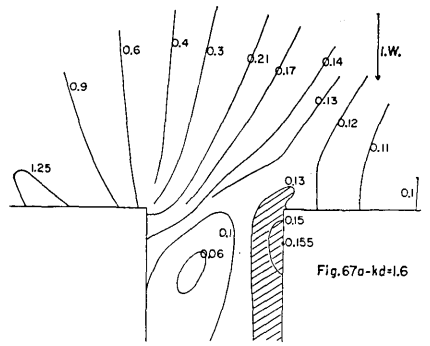

Fig. 67a. Variation of the intensity $|\zeta_{ec}|$ denoting the effect of the right corner upon the wave diffracted from the left corner for $kd=1.6$.*

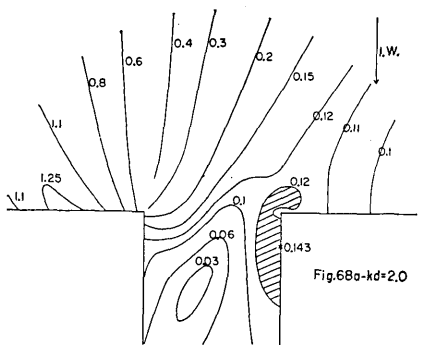

Fig. 68a. Variation of the intensity $|\zeta_{ec}|$ denoting the effect of the right corner upon the wave diffracted from the left corner for $kd=2.0$.*

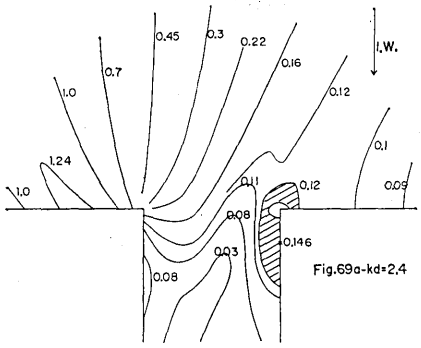

Fig. 69a. Variation of the intensity $|\zeta_{ec}|$ denoting the effect of the right corner upon the wave diffracted from the left corner for $kd=2.4$.*

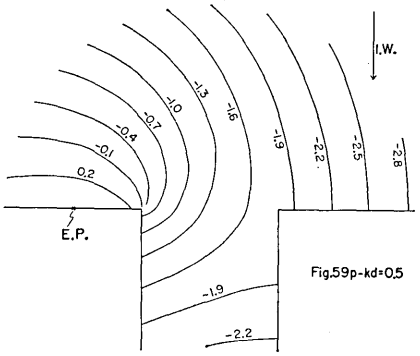

Fig. 59p. Variation of the phase arg ζ_{ec} denoting the effect of the right corner upon the wave diffracted from the left corner for $kd=0.5$.**

* See the footnote of Figs. 2a-5a.
** See the footnote of Figs. 31p-34p.

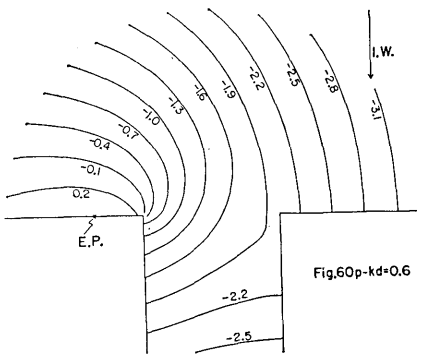

Fig. 60p. Variation of the phase arg ζ_{ec} denoting the effect of the right corner upon the wave diffracted from the left corner for $kd=0.6$.**

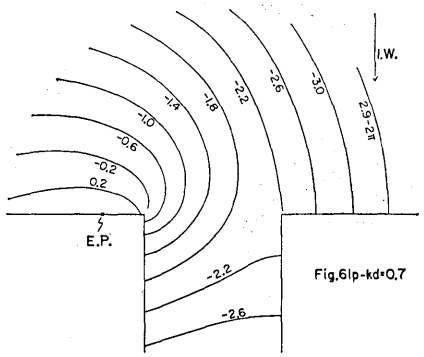

Fig. 61p. Variation of the phase arg ζ_{ec} denoting the effect of the right corner upon the wave diffracted from the left corner for $kd=0.7$.**

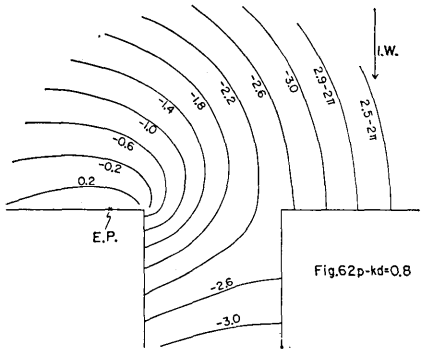

Fig. 62p. Variation of the phase arg ζ_{ec} denoting the effect of the right corner upon the wave diffracted from the left corner for $kd=0.8$.**

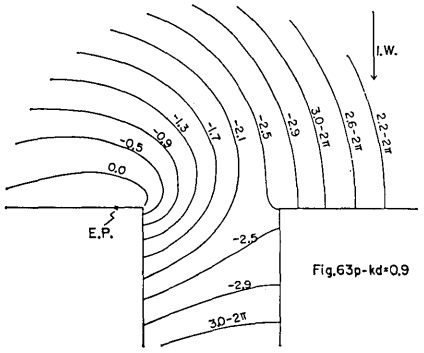

Fig. 63p. Variation of the phase arg ζ_{ec} denoting the effect of the right corner upon the wave diffracted from the left corner for $kd=0.9$.**

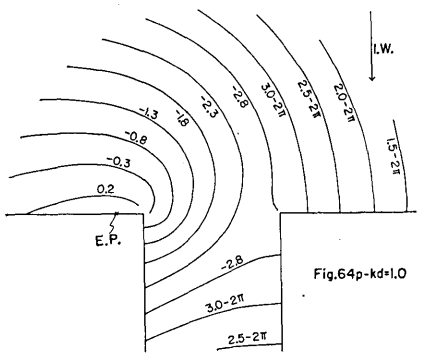

Fig. 64p. Variation of the phase arg ζ_{ec} denoting the effect of the right corner upon the wave diffracted from the left corner for $kd=1.0$.**

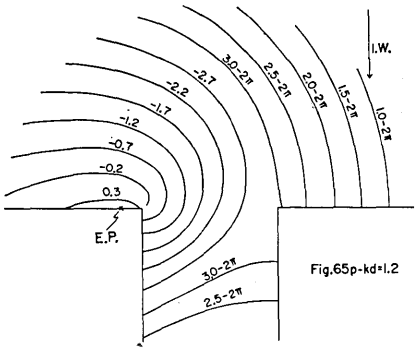

Fig. 65p. Variation of the phase arg ζ_{ec} denoting the effect of the right corner upon the wave diffracted from the left corner for $kd=1.2$.**

** See the footnote of Figs. 31p-34p.

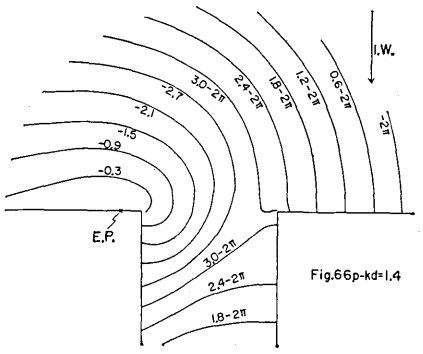

Fig. 66p. Variation of the phase arg ζ_{ec} denoting the effect of the right corner upon the wave diffracted from the left corner for $kd=1.4$.**

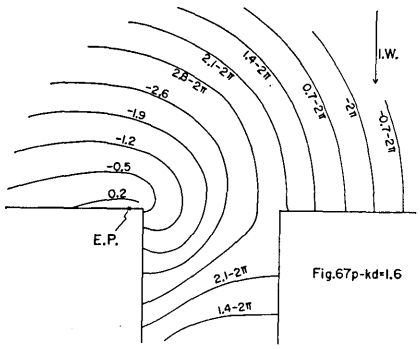

Fig. 67p. Variation of the phase arg ζ_{ec} denoting the effect of the right corner upon the wave diffracted from the left corner for $kd=1.6$.**

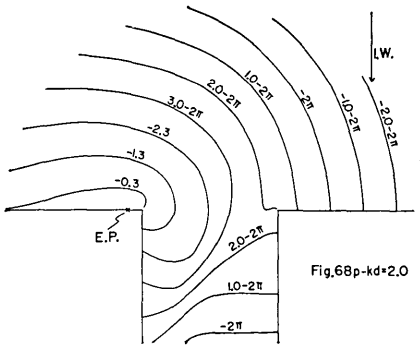

Fig. 68p. Variation of the phase arg ζ_{ec} denoting the effect of the right corner upon the wave diffratced from the left corner for $kd=2.0$.**

latter.

In Figs. 59a to 69a (the amplitude variation), the wave of high intensity appears inside the canal along the right-hand bank, which is characterized by the shadow. Inspection of the above shadowed region through Figs. 59a to 69a shows that the high intensity along the right-hand bank amounts to about 0.3 of the amplitude of the incident wave ($=1.0$) for $kd=0.5$ (Fig. 59a) to decrease gradually down to about 0.2 for $kd=1.0$ and further about 0.1 for $kd=2.0$. The shaded region of the high intensity arrives at the left bank extending from the right one for small kd (say Figs. 59a to 62a), while the above region continues diminishing with the increase of kd (Figs. 63a to 67a) until the high intensity is limited to the nearby waters of the right-hand corner of the estuary (Figs. 68a and 69a).

As for the phase variation (Figs. 59p to 68p), the diffracted waves from the left corner start at the point along the coast slightly away from the very point of the corner to be propagated toward the right corner, in which some of them advance along the coast in the open sea and the others collide with the right bank of the canal to cause the high wave there.

** See the footnote of Figs. 31p-34p.

The direction of the diffracted wave at the midpoint of the mouth of the estuary is shown in Fig. 69p for the change of kd. The figure denotes that the advancing component of the wave toward the inside of the canal is more conspicuous for smaller kd than for larger kd, suggesting the strong inflow of the wave to the canal for small kd. This feature is consistent with the behavior of the emitting point of the secondary wave reflected along the bank of the canal, that is to say, the larger departure of the emitting point from the corner of the estuary toward the inside of the canal for smaller kd (refer to Section 5).

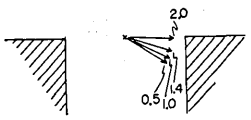

Fig. 69p. Direction of the propagation of the diffracted wave, from the left corner, at the midpoint of the mouth of the estuary. The arrows denote the direction of the wave with the numerals showing the values of kd.

8. Reflection of the Diffracted Wave around the Right-angled Corner

When the incident wave invades the right-angled corner (refer to Fig. 70), the wave is diffracted around the corner toward the leeward waters. The diffracted wave arrives at the leeward boundary to cause a secondary reflection. In order to examine the above-mentioned secondary reflection, the following procedure is devised. Let ζ_{rc} and ζ_{sbw} be the wave heights around the right-angled corner and the single breakwater wing for the invasion of a train of the periodic waves $\exp(+i\omega t+iky)$ (ω, k, t and y: the angular number, wave number, time variable and the y-component of the cartesian coordinate). The secondary reflected wave around the right-angled corner (ζ_{rdf}) is well expressible by the subtraction of ζ_{sbw} from ζ_{rc}, i.e.,

$$\zeta_{rdf} \fallingdotseq \zeta_{rc} - \zeta_{sbw} , \qquad (4)$$

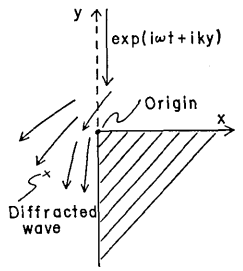

Fig. 70. Geometry of the right-angled corner.

where ζ_{rc} and ζ_{sbw} are given by equation (17) of the last paper concerning the wave around the estuary (*Momoi*, 1968b) and equation (1) of the paper relevant to the long wave around the breakwater (*Momoi*, 1969). Equation (4) is illustrated in Fig. 71.

Using equation (4), the calculation is carried out for the secondary wave in the range $kd=0$ to 15.0, the results of which are presented in Figs. 72a to 74a for the amplitude and Figs. 72p. to 74p for the phase. In Figs. 72a to 74a, the region of the amplitude over 20 per cent of that of the incident wave is expressed by the shaded part. For the

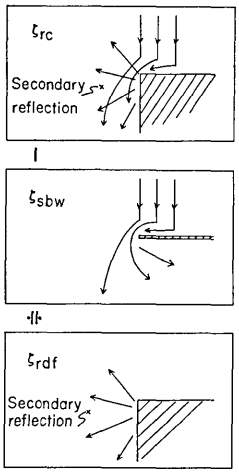

Fig. 71. Schema of equation (4).

comparatively long wave, the shaded part extends to the wider area of the leeward waters (see Fig. 72a). As the wave-length of the incident wave decreases, the above shaded area continues diminishing to the narrower band along the leeward coast (see Figs. 73a and 74a). According to the figures of the phase (Figs. 72p to 74p), the reflected wave from the leeward coast is clearly found, which is directed primarily to the leeward waters. Some of the above reflected wave advances toward the windward waters to cause the phase retardation of the RST wave near the corner of the estuary (see Section 3 discussing the RST wave around the estuary). The above phenomenon is illustrated in Fig. 75.

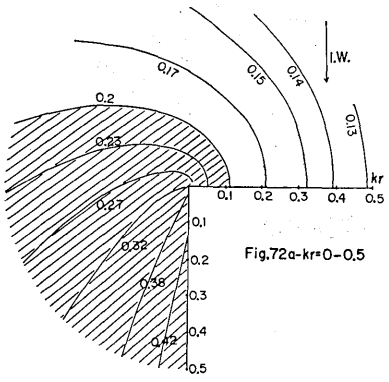

Fig. 72a. Variation of the amplitude of ζ_{rdf} for $kr=0\sim0.5$.*

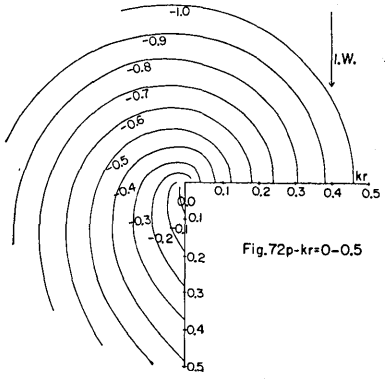

Fig. 72p. Variation of the phase of ζ_{rdf} for $kr=0\sim0.5$.*

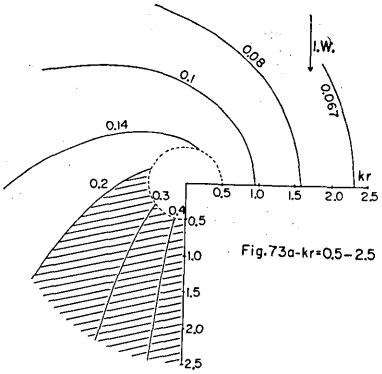

Fig. 73a. Variation of the amplitude of ζ_{rdf} for $kr=0.5\sim2.5$.*

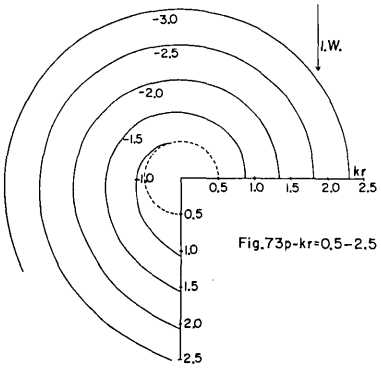

Fig. 73p. Variation of the phase of ζ_{rdf} for $kr=0.5\sim2.5$.*

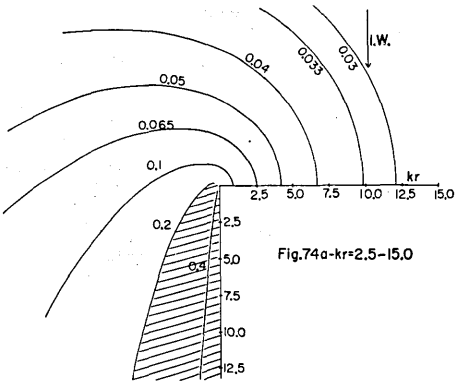

Fig. 74a. Variation of the amplitude of ζ_{rdf} for $kr=2.5\sim15.0$.*

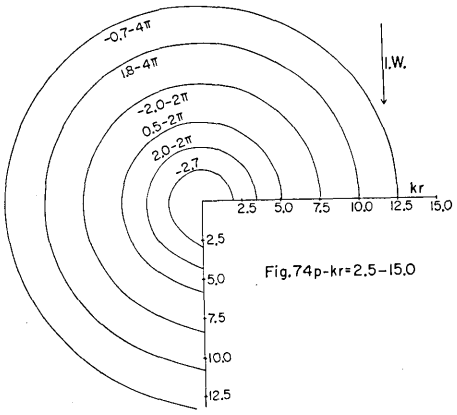

Fig. 74p. Variation of the phase of ζ_{rdf} for $kr=2.5\sim15.0$.*

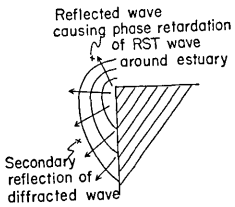

Fig. 75. Secondary reflection of the diffracted wave around the right-angled corner.

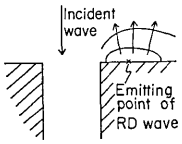

Fig. 76. Location of the emitting point of RD wave.

9. Note on the Emitting Point of RD Wave

In Section 5 of the fourth paper (*Momoi*, 1968a), we have discussed that the emitting point of the RD wave (reflected and diffracted wave) around the estuary is located at a point slightly apart from the very point of the corner along the coast facing the open sea (see Fig. 76). The possible causes of the above departure are (i) the diversion of the invading wave to the coast near the mouth of the estuary, (ii) the secondary reflection along the coast of the diffracted wave from the other corner and (iii) the influence of the secondary reflection of the diffracted wave from the canal. The above three possible causes are illustrated in Fig. 77. If the above first two reasons, i.e., (i) and (ii) should be accepted as the primary causes, the same feature—the departure of the emittng point of the RD wave—would have to appear for the model

* See the footnote of Figs. 2a-5a.

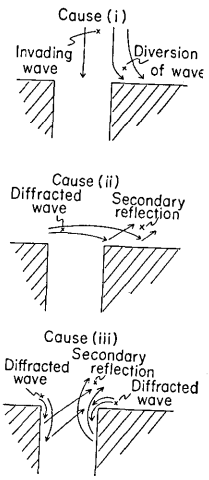

Fig. 77. Possible causes of the departure of the emitting point of RD wave.

of the double breakwater wings (the case of the normal incidence of the incident wave). As already mentioned in the fifth work concerning the estuary (*Momoi*, 1968b), we have found that, after the numerical experiment, the emitting point of the RD wave for the breakwater is the very point of the terminus of the breakwater wing (see Fig. 25 of the above paper) instead of the point slightly distant. In the computation of the RD wave around the single right-angled corner in the above work (see Section 6 of the paper (*Momoi*, 1968b)), it is found that the RD wave starts at the point slightly distant from the corner (see Fig. 40b) even for the single right-angled model. These facts might eliminate the possibility of (i) or (ii) as the primary cause. And further, according to Section 6 (Effect of the Banks of the Canal), the reflected wave from the canal arrives again at the coast exposed to the incident wave in not negligible order.

We have now arrived at the conclusion that the influential cause of the departure of the emitting point of the RD wave from the corner point is (iii) illustrated in Fig. 77, though the other factors might contribute to it to a somewhat lesser degree.

References

Momoi, T., 1965a, A Long Wave in the Vicinity of an Estuary [I], *Bull. Earthq. Res. Inst.*, **43**, 291-316.

Momoi, T., 1965b, A Long Wave in the Vicinity of an Estuary [II], *Bull. Earthq. Res. Inst.*, **43**, 459-498.

Momoi, T., 1966, A Long Wave in the Vicinity of an Estuary [III], *Bull. Earthq. Res. Inst.*, **44**, 1009-1040.

Momoi, T., 1967a, A Long Wave around a Breakwater [I], *Bull. Earthq. Res. Inst.*, **45**, 91-136.

Momoi, T., 1967b, A Long Wave around a Breakwater [II], *Bull. Earthq. Res. Inst.*, **45**, 749-783.

Momoi, T., 1968a, A Long Wave in the Vicinity of an Estuary [IV], *Bull. Earthq. Res. Inst.*, **46**, 631-650.

Momoi, T., 1968b, A Long Wave in the Vicinity of an Estaury [V], *Bull. Earthq. Res. Inst.*, **46**, 1237-1268.

Momoi, T., 1969, A Long Wave around a Breakwater [VI], *Bull. Earthq. Res. Inst.*, **47**, 165-184.

21. 河口近傍における長波について [VI]

地震研究所　桃　井　高　夫

本報告に論じられている内容は次のごとくである．第 3 節において RST（合成）波，第 4 節において RD（反射回折）波，第 5 節において 2 次的な反射，第 6 節において河口水路の影響，第 7 節において回折波に対する反対側の河口隅の影響，第 9 節において RD 波の出発点についての論で，以上はすべて河口近傍の長波についての論議である．更にまた，単一の直角隅角部の回折波の 2 次的反射が第 8 節において調べられている．

得られた結論のうちで著しいことは次のごとくである．

(i) 河口水路の横モードは $kd=\pi$ (k: 進入波の波長，d: 河口水路の幅の半分長) のときもっとも大きくなり（共鳴モードを意味する），その量は約 0.5（進入波の振幅を 1.0 として）に達する．

(ii) kd が小さいとき，河口近傍における回折波の 2 次的反射波は 2 種類にわかれる．一つは河口近くの海岸において広海に反射する波，もう一つは水路の堤で水路内に反射する波である．

(iii) 河口近傍の回折波の 2 次的な反射波のうちで，回折波が回折をうけた海岸の直接背後の水路堤よりの 2 次反射は他の 2 次反射より大きく約 4 あるいは 5 倍に達する．